# COMPUTER CONTROL OF A HYDRAULIC PRESS BRAKE

BY

John Alexander Lane
B.Sc. (Mechanical Engineering), 1988
University of New Brunswick

A THESIS SUBMITTED in PARTIAL FULFILLMENT OF

THE REQUIREMENTS FOR THE DEGREE OF

MASTER OF APPLIED SCIENCE

in

THE FACULTY OF GRADUATE STUDIES

Department of MECHANICAL ENGINEERING

We accept this thesis as conforming

to the required standard

## UNIVERSITY OF BRITISH COLUMBIA

APRIL, 1994

In presenting this thesis in partial fulfilment of the requirements for an advanced degree at the University of British Columbia, I agree that the Library shall make it freely available for reference and study. I further agree that permission for extensive copying of this thesis for scholarly purposes may be granted by the head of my department or by his or her representatives. It is understood that copying or publication of this thesis for financial gain shall not be allowed without my written permission.

(Signature)

Department of MECHANICAL ENGINEERING

The University of British Columbia
Vancouver, Canada

Date 25 APRIL 1994

# Abstract

Hydraulic press brakes are widely used in industry to form sheet metal into various shapes using bending operations. When the press brake is controlled by a Computer Numerical Control (CNC) unit, the desired bend can be achieved without the use of mechanical gages or manual adjustments, leading to increased flexibility and accuracy in the manufactured components.

In this thesis, a single axis hydraulic press brake is retrofitted for dual axis CNC control. The ram is positioned using two parallel hydraulic cylinder type actuators. One servo-valve and amplifier is dedicated to each actuator so that the motion of each axis can be independently controlled by the CNC unit. Each actuator is instrumented with linear optical encoders which provide feedback for closed-loop servo position control. The hydraulic system is modified to provide constant pressure fluid power to the servo-valves. An accumulator is used between the pump and the valves to suppress pressure fluctuations. Pressure transducers are integrated into the ports of the actuator to monitor the pressure during the operation of the press.

The dynamics of the hydraulic servo system, including the valves, actuators and the ram are modeled. A non-linear model, which includes the influences of piston position, is presented. A simplified model is shown to be adequate provided that the practical ranges of the piston position is considered. The mathematical model is used to experimentally determine the dynamics using parametric identification techniques. The well-damped system is approximated by a first order system with substantial delay between the servo-valve amplifier command and the actuator piston motion. A readily-available CNC system is retrofitted to the press brake and a delay compensating pole-placement digital control system is developed and implemented for the independent

control of two actuators. The performance of the system is evaluated for a series of forming operations.

This thesis provides basic guidelines for the design and analysis of hydraulically actuated CNC presses.

# Table of Contents

# List of Tables

# List of Figures

# Acknowledgments

# Chapter 1

# Introduction

A hydraulic press brake is a machine tool used to form bends in metal plate or sheet. In production, a typical press brake is setup to perform a single bend in a batch of similar components. The bend angle is set by trial and error using an adjustable mechanical stop. This setup requires several attempts and is only useful for one bend angle.

By comparison, Computer Numerical Control (CNC) press brakes use closed-loop position control which improves precision and simplifies the setup such that only one trial bend is needed. Since setup information is stored digitally, CNC press brakes can be programmed to perform a number of different bends at any particular instant in time.

In this thesis, a single axis hydraulic press brake is retrofitted for dual axis CNC control. The focus of this thesis is the servo system used to position the forming tools. The objective of this work is two fold:

- to reduce uncertainty during the design stage by investigating models used to represent the system dynamics
- to investigate ways of improving system performance in the face of unexpected design shortcomings

In this work, a hydraulic servo positioning system is designed, modeled and analyzed. A hydraulic supply for servo positioning system is designed and implemented. High performance servo-valves are mounted to the existing actuators. Mechanical modifications are made to allow independent actuator motion. A position feedback

system utilizing linear optical encoders is designed and implemented. The dynamic characteristics of the system are experimentally verified using system identification techniques. Based on the results of these experiments, a delay-compensating pole-placement control scheme is chosen and implemented. The performance of the CNC press brake is evaluated.

A survey of both research and industrial literature concerning the brake-forming operation, press-brakes, hydraulic system modeling and relevant automatic control theory is presented in Chapter 2.

Chapter 3 describes the work required to convert the manually controlled press brake to one capable of computer control. Details of the hydraulic and mechanical designs are presented and a description of the electrical hardware used for control.

In Chapter 4, models used to represent the dynamics of the hydraulic positioning system are presented and applied. An alternate actuator compliance model is developed and investigated. A summary of general recommendations for modeling is given.

Chapter 5 describes the system identification experiments conducted on the position control system. Results of step response, frequency response and parametric identification tests are presented and discussed. A summary of conclusions for control is presented.

The delay-compensating, pole-placement control scheme is described in Chapter 6. A simplification to the control law is developed. The performance of the positioning system is evaluated in terms of system response, dead-band, following error, and stiffness. The results are presented and discussed.

Finally, Chapter 7 is a summary of conclusions arrived at through this work. Recommendations for future work are suggested.

# Chapter 2

# Literature Survey

## 2.1 The Brake Forming Process

"Brake forming is a method of forming straight-line bends in sheets and plates" [1].
In a brake forming operation a sheet metal workpiece is positioned between a punch and a
die. The bend is formed as the punch penetrates the die. Although variations exist, there
are two fundamental types of brake forming operations. When the punch bottoms the
work piece in the die the operation is known as *coining* or *bottom bending*. When the
punch does not bottom the work-piece in the die the operation is known as *air-bending*
[2]. The brake forming process is illustrated in figure 2.1.
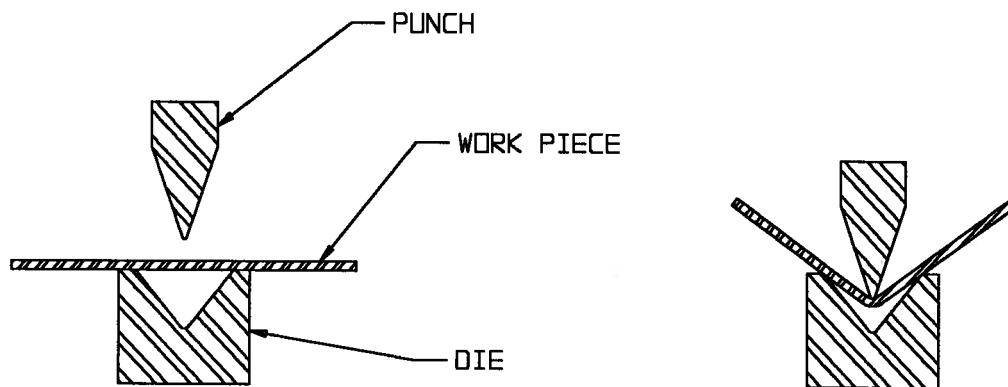
Figure 2.1. The brake forming process.

In the ideal bottom bending operation, the yield stress of the work piece material is
induced throughout out the area of the bend, causing the work piece to take the shape of

the punch and die. While bottom bending generally produces the best quality bends, it requires very high actuation forces and specially mated tooling for each angle of bend [3]. In an air bending operation, the angle of bend is determined by the amount of punch penetration. Therefore, air bending operations do not require specially mated tooling. Furthermore, since the yield stress of the material is not induced throughout the area of the bend, the actuation force required is two to five times lower than that required by bottom bending [2]. Because of this inherent advantage, automation efforts in brake forming have focused on the air-bending operation [4]. However, the cost of not inducing the yield stress of the material throughout the area of bend is that a certain amount of elastic deformation remains at the final punch penetration. This elastic deformation causes the work piece to 'spring-back' when the punch is withdrawn from the die. Compensation models, which are capable of approximating *spring-back* given the desired bend angle and the material thickness, are frequently used [5].

## 2.2 Hydraulic Press Brakes

Brake forming operations are performed on machines known as press brakes. A technical illustration of the Accurpress press brake used for this project is shown in figure 2.2. This machine is typical of those utilized in the industry. The fundamental components of the press brake are depicted.

The punch is clamped to a large ram which is positioned by two hydraulic actuators. The actuators are driven in parallel by a single or multistage solenoid operated valve system. Usually, the hydraulic circuit has provisions for two speeds: one for rapid positioning and one for the forming operation. The die is fixed to the press bed. The positioning system controls the amount the punch penetrates the die. Due to the extremely high forces applied, the ram gibbing is not sufficient to hold the punch parallel

to the die. As a consequence, press brakes use an auxiliary system to ensure tooling is properly oriented. The fundamental differences between manually operated press brakes and automated ones lie in these two systems, which ensure appropriate positioning and orientation of the punch with respect to the die.
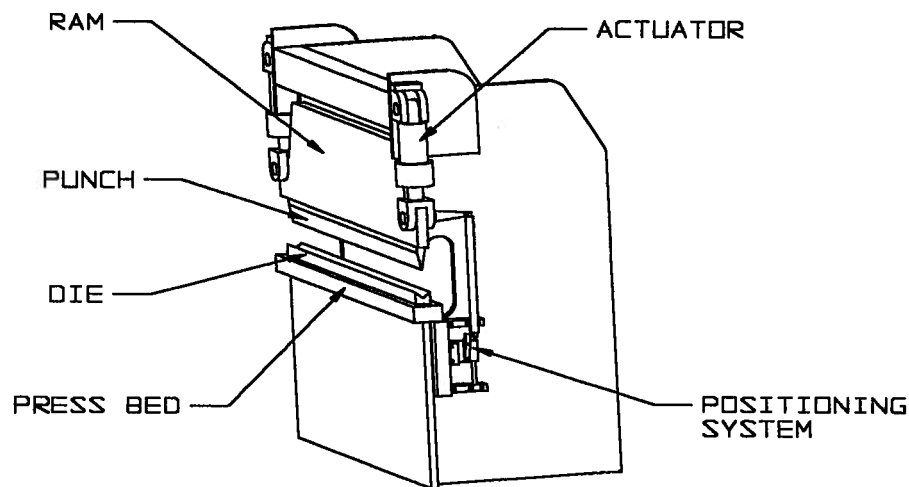


Figure 2.2. A typical press brake.

With manually operated press brakes, the positioning system and the orientation system are distinct mechanisms. The orientation mechanism may consist of a stiff mechanical device or a sensitive hydraulic feedback circuit adjusted to minimize tilt of the ram during asymmetrical loading conditions. Typically the positioning system consists of a calibrated adjustable stop and an electronic switch which triggers a solenoid driven hydraulic valve. When flow to the actuator is arrested or reversed, the punch penetration is limited. The accuracy of this system is dependent upon the sensitivity of the switch as well as the condition of the hydraulic system. All hydraulic systems are subject to variations in fluid viscosity and bulk modulus. These variations can cause significant deviations in the final punch penetration over the run of a batch of parts.

On a two-axes CNC press brakes the orientation as well as the positioning tasks are handled by an integrated position control system. The flow of hydraulic fluid to each actuator is controlled by two independent precision single or multistage spool valves. The relative position of each actuator is measured by a high resolution position transducer. The movement of each actuator or axis is controlled by a digital feedback control scheme. Typically, CNC press brakes use gibbing which allows some tilting of the ram but the relative orientation of the tooling is ensured by linking each axis at the control level. Because these systems use feedback control the positioning is much less affected by changes in the state of the hydraulic fluid. The benefits of computer-controlled positioning systems are many.

For a given batch of parts requiring the same bend angle, the setup procedure for a press brake involves three steps. First, the punch and die are mounted and adjusted to be coplanar. Next, the clamping mechanism is adjusted to ensure the forming edges are parallel. Finally, the positioning mechanism is set to give the desired bend. Trial and error testing of the forming operation is performed until the finished bends are within tolerance. With manually operated press brakes, this procedure is repeated many time, not usually less than three [2]. By comparison, the setup procedure for CNC press brakes is much simpler. A tooling offset reference is set by bottoming the punch in the die, and a predictive model is used to calculate the desired punch penetration. After a test workpiece has been bent, the error between the desired work piece and the test piece is entered into the positioning controller and then the press brake is ready to form parts. In this way CNC press brakes require much less setup time. Furthermore, once a series of bends have been tested and calibrated, the CNC press brake can readily switch between bends with no extra setup time.

## 2.3 Hydraulic Supply Systems

Hydraulic servo-actuators used for positioning systems require constant pressure supply systems. Although constant supply pressure under varying loading conditions is difficult to achieve, Ahmed and Asok [6] have reported that slight (<10%) fluctuations in the supply pressure have little effect on the response of the servo-actuator. In order to achieve this constraint, some consideration must be given to the design of the hydraulic supply system.

Systems that supply fluid power to hydraulic systems can be classified into one of two categories: constant delivery systems or variable delivery systems. In the simplest form, a constant delivery system designed to provide constant pressure can consist of a fixed displacement pump and a pressure relief valve (PRV). In order to maintain a relatively constant system pressure the pump would supply a constant flow of fluid to the supply line and the PRV. Whatever flow is not used by the servoactuator would pass through the PRV at maximum pressure drop. Although this type of system is inexpensive to implement, the cost of providing the maximum flow rate at the system pressure is two fold; the overall efficiency of the system is low, and the quantity of heat generated by this low efficiency can breakdown the hydraulic fluid. For these reasons, constant delivery systems are rarely used in servoactuator applications.

Variable delivery systems have the advantage of being able to provide only enough flow to satisfy the requirements of the servo-actuator while accommodating some internal leakage. Depending on the type of pump being used, variable delivery flow can be achieved in one of two ways. If a fixed displacement pump is used, the pump would provide flow to a hydraulic accumulator which in turn would supply the servo-actuator.

When the system pressure reaches the desired pressure, the pump would be shut off until the system pressure falls below a prescribed lower pressure limit. While this type of system is more efficient than a constant delivery system, a compromise must be made between the frequency at which the pump is cycled and the maximum pressure fluctuation allowed.

Systems employing variable displacement pumps use pressure feedback to continuously vary the flow to track the desired system pressure. The fundamental components of a pressure-compensated variable delivery hydraulic supply system are: a variable displacement pump with pressure feed-back, a hydraulic accumulator, and a check valve (figure 2.3). In this system, the pump utilizes an internal spool valve to control the angular displacement of the swash plate. As the swash plate angle increases, so does the flow delivered from the pump. When the pressure in the supply line deviates from the desired system pressure, the control valve adjusts the output flow-rate to maintian the desired system pressure. Since the response time of this type of pump is generally slower (50-120ms) than response time of a typical servovalve (4-20ms) an accumulator is used to satisfy the flow requirements while the pump is responding to a demand for more flow. Although these systems are generally more expensive than the systems described previously, they are capable of providing the smoothest supply pressure with a minimum of pressure fluctuation. For this reason, they are the most common supply system used with precision servoactuators.
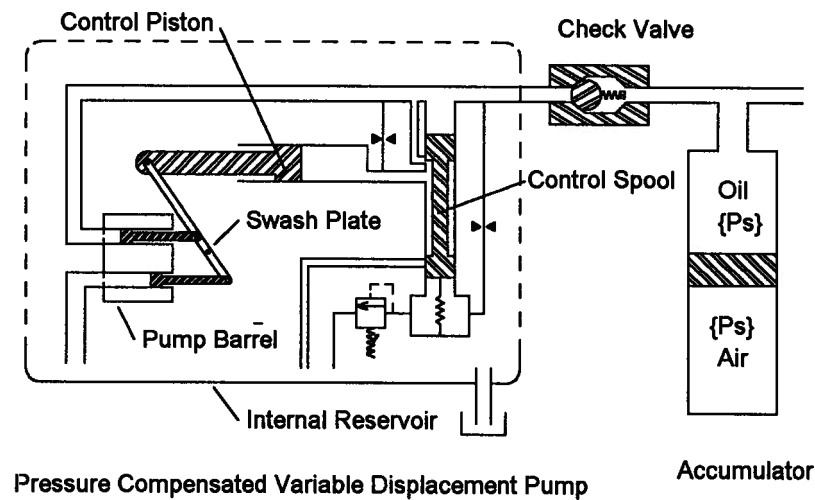
**Figure 2.3.** Pressure Compensated Variable delivery hydraulic supply.

## 2.4 Cylindrical Hydraulic Servo Actuators

A schematic diagram of a hydraulic servo-actuator used for CNC press brakes is presented in figure 2.4. The load is connected to the output shaft of a hydraulic cylinder. The cylinder consists of two chambers: the piston-side chamber and the rod-side chamber. For high performance systems, flow to each chamber of the cylinder is typically controlled by a high-precision multistage critically-centered spool valve often called a servo-valve. An electronic amplifier supplies a command signal to the valve. The output velocity of the load is proportional to the servo-valve command signal. The characteristics of the main components which make up these servo-actuators, the loaded actuator and the servo-valve have been thoroughly investigated.[6-16].

Previous investigations of cylindrical hydraulic servo systems have found that very little viscous damping is attributable to the actuator[7,17]. When the compliance of the hydraulic fluid within the actuator is considered, a symmetrical actuator at mid-stroke behaves as an under damped second order system [13]. Asymmetrical actuators can be modeled by a third order system [11]. Depending on the gibbing or guide ways used for the system, significant amounts of Coulomb damping may also be present [18].

The dynamics of a two-stage servo-valve can be represented by a simple lag due to the torque motor driving the primary stage combined with a quadratic lag due to the dynamics of the secondary stage flow controlling spool. Often the dynamics of the flow controlling spool are fast enough to render them insignificant. The flow through the servo-valve is proportional to the valve opening and the square root of the pressure drop across the open port.
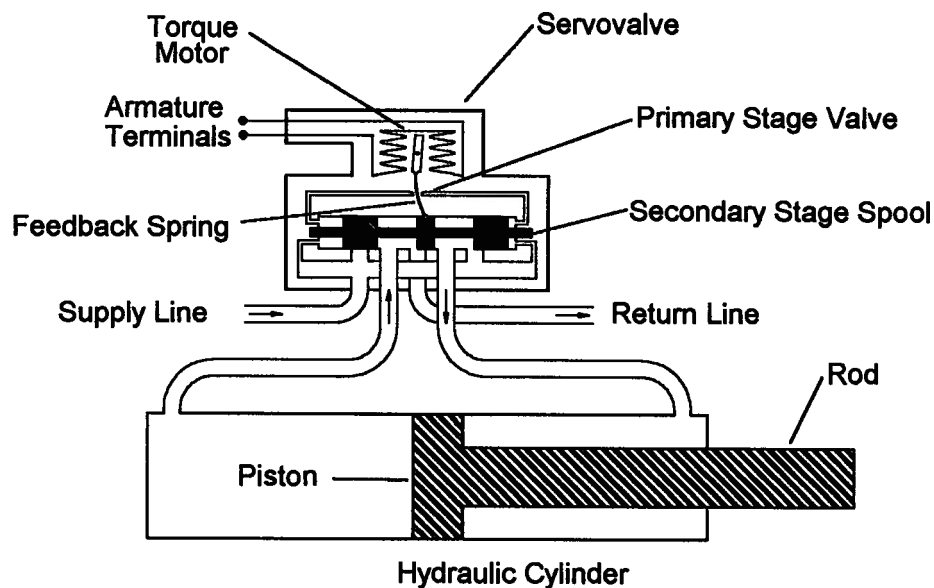


Figure 2.4. Components of a hydraulic servo-actuator.

The fundamental difficulties in controlling servo-actuators stem from five phenomena:

    i) the nonlinear pressure/flow relationship for the flow through the servo-valve

    ii) the inherent lack of viscous load damping

    iii) the presence of significant Coulomb damping

    iv) varying actuator compliance and

    v) variation of characteristics of hydraulic system.

Although the non-linear pressure flow relationship can have significant affect on the large signal response of the servo-actuator, it is generally considered insignificant for typical operating control signals. Therefore, it is common practice to linearize the flow characteristic about the null operating point, where the spool is centered and the ports closed. This represents the worst-case scenario for closed loop stability because the valve gain is highest and the flow damping is lowest. Alternate methods of analysis have been developed to predict the frequency response of the system which varies with the amplitude of the input signal [13].

In cases where the response of the control valve is much faster than the response of the loaded actuator, significant research effort has been expended to overcome the lack of viscous damping [9,17,19]. Some of the earliest schemes to improve damping involved the introduction of laminar leakage across the chambers of the actuator. These systems were simple to implement but reduced the stiffness and efficiency of the actuator. Transient flow networks, unlike the leakage techniques, were non-dissipative but they were difficult to tune and reduced actuator stiffness. Hydromechanical feedback mechanisms were developed which added the required damping and increased the actuator stiffness, but these systems required precision manufacturing operations which were specific to each valve/actuator/load combination. The cost and flexibility of these

methods were improved when electronic feedback of acceleration and pressure signals replaced hydromechanical feedback. Modern digital controllers are capable of addressing this problem in a number of ways, the most common being pole-placement control schemes [20].

The presence of Coulomb damping has the combined effect of reducing the oscillatory nature of the system response while also contributing to the steady state error. To compensate for the absence of viscous damping, early analyses made attempts to model Coulomb damping as a theoretical viscous equivalent [11,21]. Current analyses simply treat this damping as an external force disturbance [22].

The compliance of a symmetrical hydraulic cylinder is a function of the bulk modulus of the hydraulic fluid and the ratio of oil volume residing on each side of the piston. Since the volume ratio changes with movement of the piston, the compliance varies as well. To simplify modeling, the common practice is to linearize the compliance relation about the most compliant position. For asymmetrical actuators the change in oil volume ratio with piston movement is more pronounced. While studies have been conducted to determine the effect of changing oil volume on the frequency response and stability of simple control systems [11], typical control strategies either assume a constant value for actuator compliance, or assume the dynamics of the loaded actuator are much faster than the dynamics of the control valve [23-24].

The sources of hydraulic system performance degradation are many. In the short term, the main cause of system degradation is the change of state of the hydraulic fluid. Hydraulic fluids used in servo-actuators have two undesirable characteristics: 1) the viscosity of the fluid changes dramatically with temperature and 2) the bulk modulus (or stiffness) of the fluid changes dramatically with the quantity of dissolved gas in the fluid. Over the long term, regular wear of precision components will cause a change in the characteristics of

the system. Moreover, long term wear is accelerated in the presence of contaminates in the hydraulic fluid.

Given the existence of these phenomena, methods to insure precise position control have recently been investigated using digital adaptive control schemes. These controllers have been labeled 'switching' adaptive controllers because the control law is updated at a frequency which is an order of magnitude lower than the loop closing frequency. Typically the adaptive controller schemes either used a method of recursive least squares to identify reduced order models of the open loop system dynamics (self-tuning regulators) or identified the control law parameters directly (model reference adaptive control) [20,22]. Provisions were made to check the stability of the system and temporarily halt estimation if the input signal ceases to be 'persistently exciting' . Several implementations used an exponential forgetting factor and/or covariance matrix resetting in the recursive identification to track time varying parameters. The most common control strategy chosen was pole-placement, but adaptive optimal controllers have also been investigated [23,25].

# Chapter 3

# Modifications Required for Computer Control

This chapter describes the work done to change the press brake from a manual to CNC control.

## 3.1 Mechanical Design Modifications

### 3.1.1 Ram Gibbing

The press brake used in this project was originally designed to allow only one degree of freedom of ram movement: vertical translation. The gibbing of the press (figure
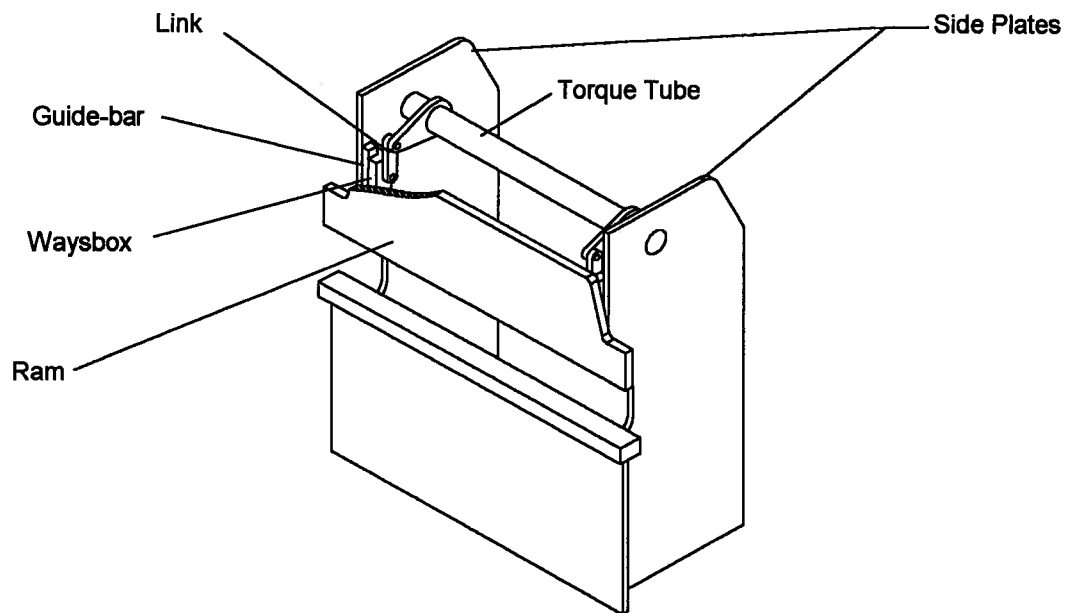


Figure 3.1. Ram orientation mechanism.

14

3.1) consisted of a pair of ways boxes which were rigidly connected to the ram, sliding on a pair of parallel guide bars, one bolted to each side plate. To maintain precise orientation of the tooling while undergoing the extreme forces of the forming process, an auxiliary device was employed. A torsional link known as a *torque tube*, was mounted between the side plates of the press. This torque tube was connected to a ways box on each side of the ram by mechanical links.
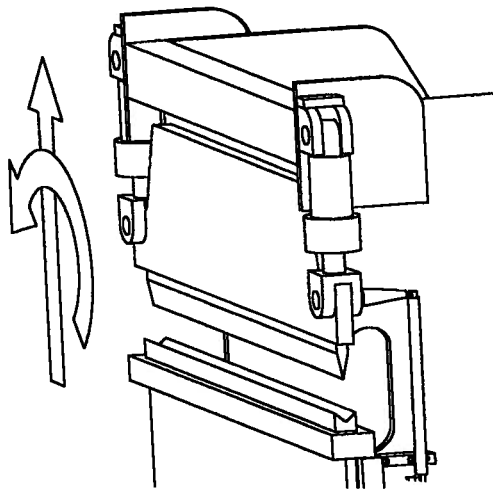


Figure 3.2. Degrees of freedom of CNC press brake.

One goal of the retrofit was to add the capability to create bends with up to three (3) degrees of trim without adjusting the tooling. This required the addition of a second degree of freedom of ram motion: rotation within the plane of the ram (figure 3.2).

In order to allow this rotation, the torque-tube was disconnected and each ways box was modified to provide guide-bar clearance. To ensure the ram remained centered between the side-plates through-out its range of motion a cylindrical sliding surface was machined in the lower ways box pad (figure 3.3). The pads were oriented such that the ram would remain centred between the guide bars.
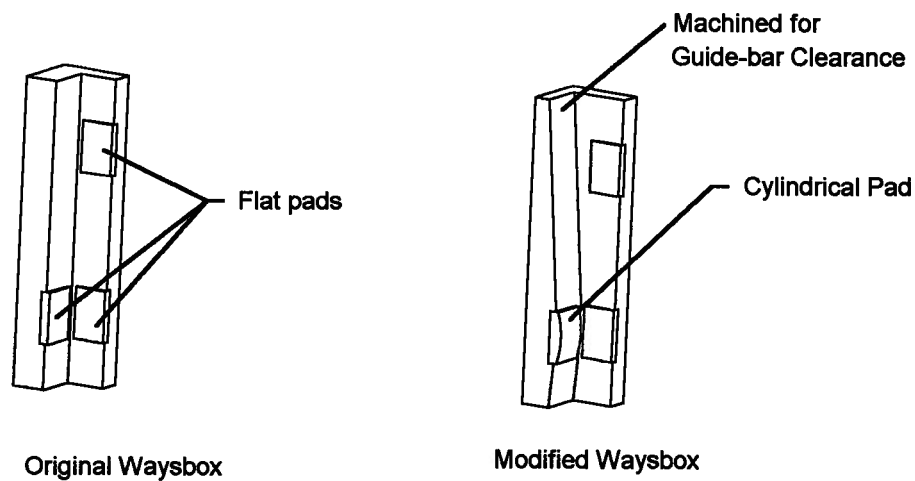
Figure 3.3. Ways box modification

## 3.1.2 Positioning System for CNC

The positioning system originally installed on the press brake is depicted in figure 3.4. This system consisted of a parallel guide mechanism which housed limit switches used to signal the *change-of-speed* and the *ram-stop* position. These switches were tripped by a moving slide which was connected to the ram by way of a tie-rod mechanism. A micrometer barrel, attached to the moving slide, was used to fine-tune the final stop position. This design was chosen to compensate for deflections which occur in the side-plates of the ram during bending. While the theoretical precision of this system was bounded by the resolution of the micrometer (0.012 mm) and the repeatability of the stop switch, the actual precision may have been worst due to the presence of a low frequency dynamic mode of oscillation with a frequency of 21 Hz.
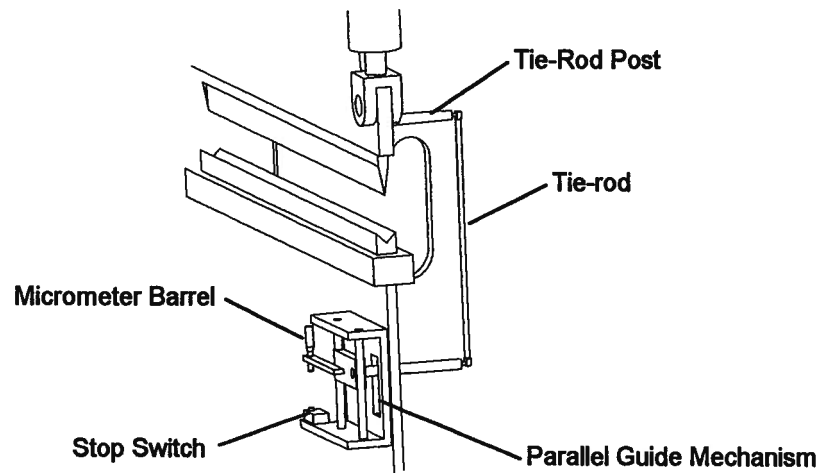
Figure 3.4. Positioning system used for manually operated press brake

## 3.1.2.1 Design Objectives

Computer controlled ram motion requires a system to measure the position and orientation of the ram. The goals for the design of this system were as follows:

- side-plate deformation compensation

- 0.01 mm position repeatability

- provisions for both position and velocity transducers

- high resonant frequency

## 3.1.2.2 Mechanical Design

In order to compensate for side-plate deformations, a design utilizing a measuring slide tie-rod connected to the ram (similar to the original system) was chosen (figure 3.5). To simplify the ram orientation task, the tie-rod posts were placed at the axes of the ram/actuator connections. High-precision ball-joints were used to connect each tie-rod to

its respective tie-rod post and slide mechanism. A lower bound on the length of the tie-rod was determined by bounding the measurement error due to tie-rod rotation.
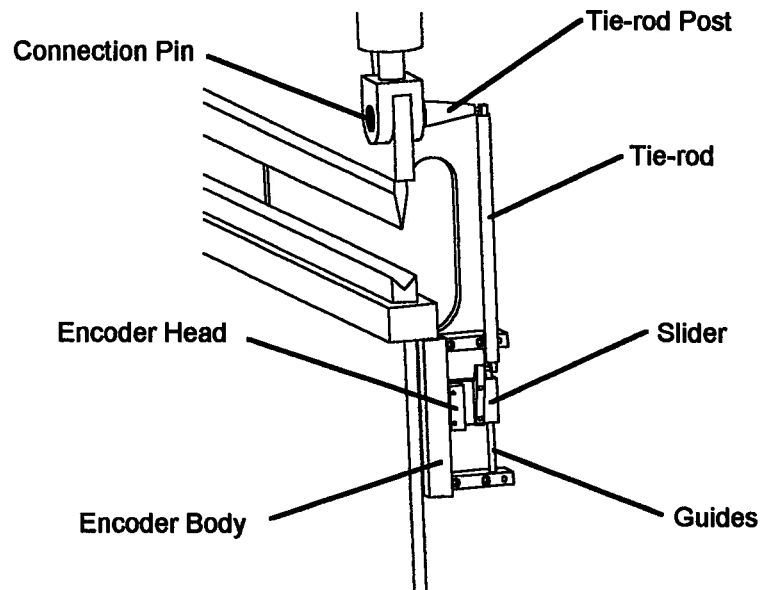


Figure 3.5. Position measurement system for CNC operation.

In order to achieve the 0.01 (mm) position repeatability, a linear encoder with a resolution of 0.005 (mm) was chosen. This encoder consists of a body which houses a fixed scale and a moving read head. The body was mounted to the press bed and the read head was attached to the translating slide of the linear guide system which was designed and manufactured in-house. The guide system utilizes a pair of cylindrical guides, one fixed, the other adjustable. This built-in adjustment capability eases alignment procedures while providing a method of preloading the guide system for greater rigidity. Provisions were made to allow the attachment of a transducer to measure the velocity of each side of the ram with respect to the bed.

The tie-rod, tie-rod posts, and the slider were designed to have high stiffness and small mass to minimize the effect of their dynamics on the feedback signal.

## 3.2 Hydraulic System

A schematic diagram of the original hydraulic system is shown in figure 3.6 Hydraulic flow was provided by two fixed displacement gear pumps: one for high pressure, the other for high flow. A pair of normally open solenoid valves, were sequenced such that both pumps provided flow during the rapid moves, but only the high pressure pump provided flow for the feed operation. A counter balance valve located in the rod-side line was used to lock the actuator during idle times.
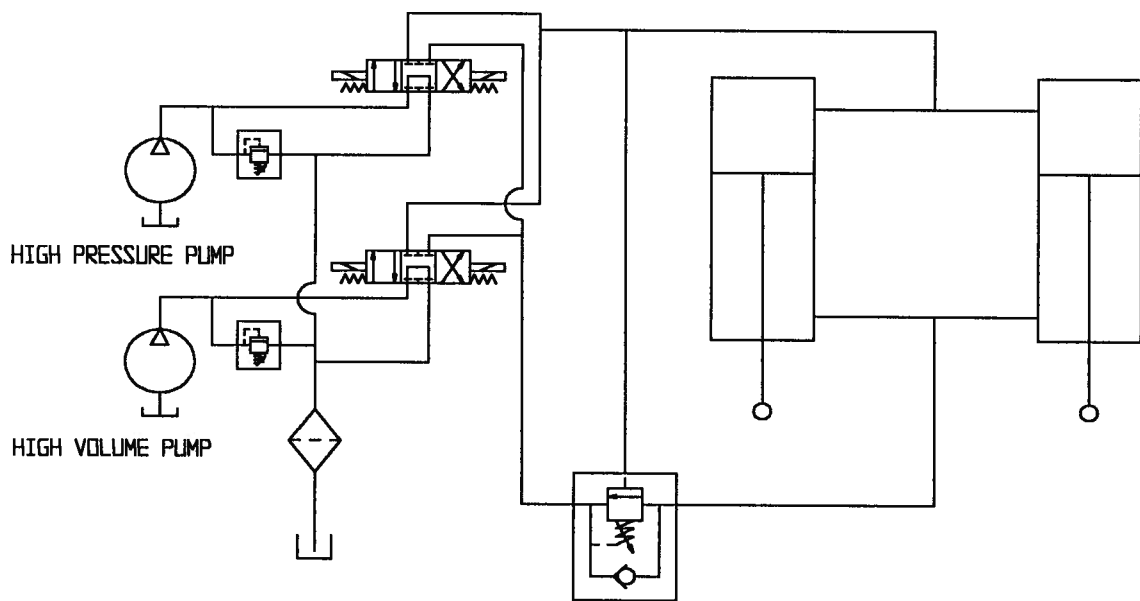


Figure 3.6. Schematic Diagram of the original hydraulic system.

For CNC press operation, the original hydraulic system was replaced by a system represented by the schematic shown in figure 3.7. A description of the components comprising this system follows.
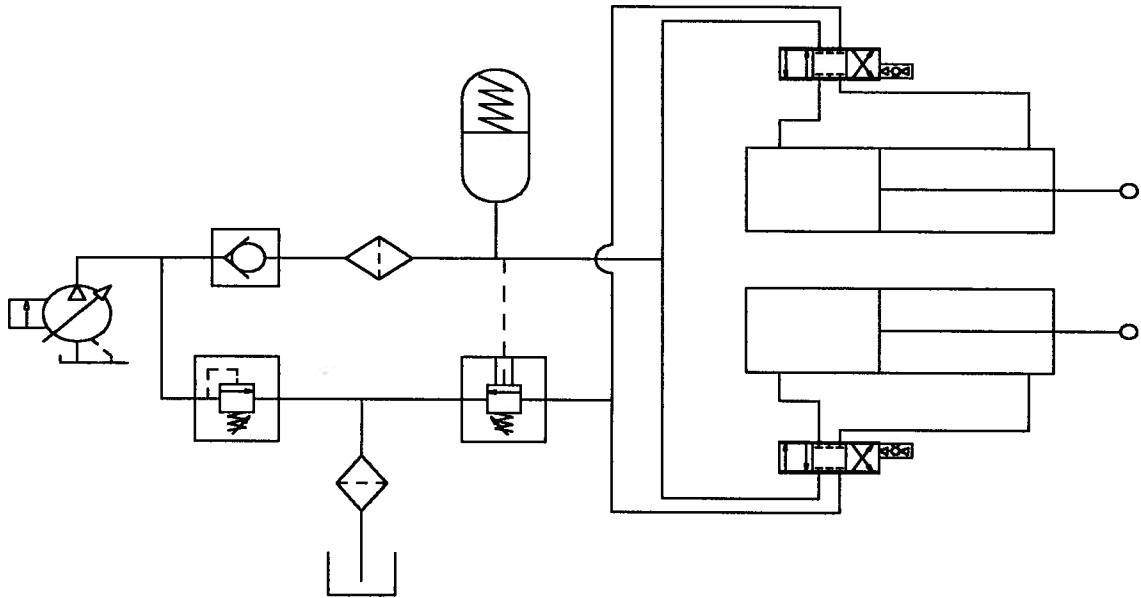
Figure 3.7. Schematic diagram of hydraulic system used for CNC operation.

## 3.2.1 Supply System

For high efficiency and good performance, a variable displacement pump with pressure feedback was chosen to deliver the hydraulic power. Since the response time of the pump was significantly slower than that of the servo-valves, an accumulator was used to keep the system pressure within 10% of the desired level. This accumulator also damps harmonic components of the pump pressure caused by the oscillating pump pistons.

A check-valve was placed between the accumulator and the pump to eliminate the possibility of the accumulator pressure driving the pump in reverse in the event of a power outage. A counter-balance valve was used to lock the system whenever the system pressure is lost.

Two filters are used to filter the fluid: a coarse low pressure filter located in the return line of the original system, and a fine, high-pressure filter in the supply line to keep metallic pump debris from reaching the sensitive pilot stage of the servo-valves.

## 3.2.2 Servo-actuator

A technical illustration of the servo-actuator used for positioning is shown in figure 3.8. The compact design of the press precluded the use of an off the shelf servo-actuator, so the original cylinders were used with only minor plumbing changes. A pair of prototype Atchley 320 servo-valves (20 g.p.m., 85 Hz bandwidth [26]) were mounted as close as possible to the ports of the original actuator.

Special in-line transducer fittings were designed and manufactured to house piezo-electric transducers capable of measuring cylinder port pressures.
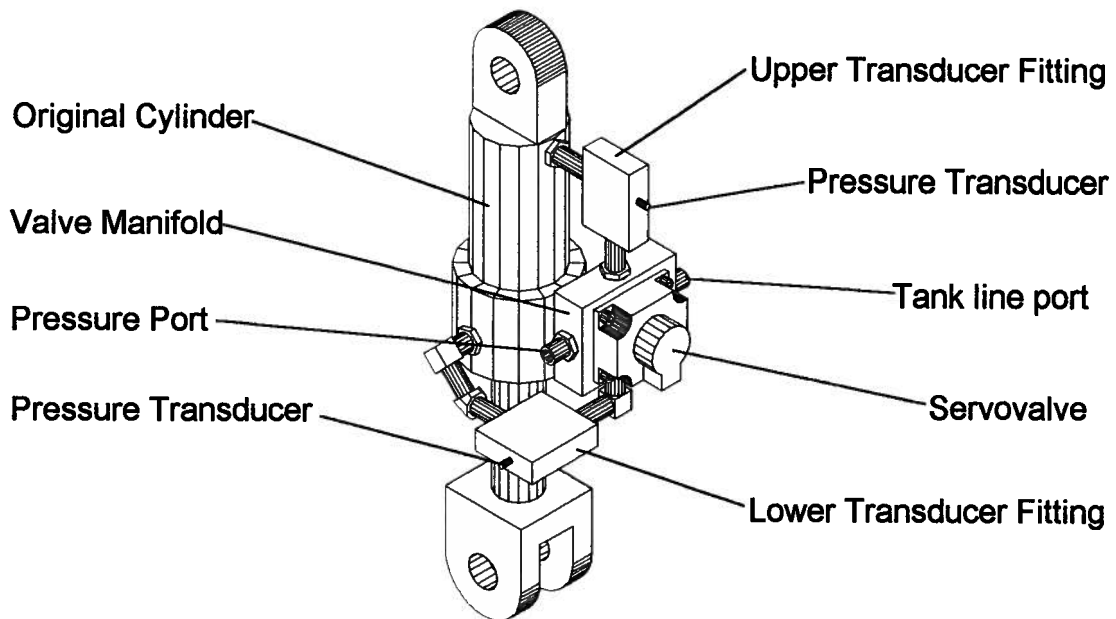
Figure 3.8. Technical illustration of servo-actuator.

## 3.3 Control Computer

The computer used to provide CNC control was the Hierarchical Open Architecture Manufacturing CNC system (HOAM-CNC) developed in-house by the CNC research group of the University of British Columbia's Mechanical Engineering department. A block diagram of this controller is shown in figure 3.9.
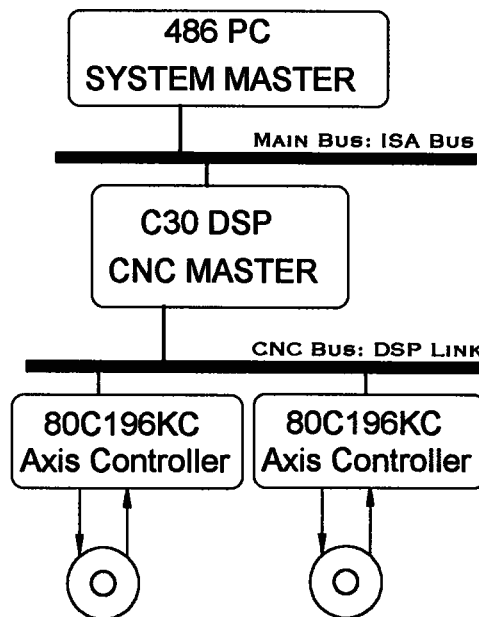


Figure 3.9. Block diagram of the Hierarchical Open Architecture Manufacturing CNC system.

The HOAM-CNC system uses a hierarchical structure to divide control tasks up between three computational systems: the system master, the CNC master, and the axis controllers. At the axis level several functions are performed: the loop is closed from a common clock pulse, some position interpolation is done, and controller status variables are updated. At the mid-level, the CNC master is used to initialize and coordinate each

axis controller. These functions have been implemented by way of a flexible task scheduling system which is also capable of high level interpolation computations and alternate functions such as data collection or on-line identification. At the top of the HOAM-CNC hierarchy is a PC based host computer which provides a user interface and mass storage. For a detailed description of the HOAM-CNC system see [27].

In order to optimize positioning performance each axis of the HOAM-CNC was modified to allow the use of a high-bandwidth, scaled control signal. The nine bit output command voltages were fed to a pair of Parker BD-98 gain amplifiers which were used to drive the servo-valves. Quadrature encoder signals from the positioning system were connected directly to inputs on the axis controllers.

# Chapter 4

# Modeling of System Dynamics

## 4.1 Introduction

In order to satisfy given performance constraints, the design of a servo-mechanism requires detailed information about how a series of individual components will perform together. Dynamic system models can provide this information if the characteristics of each component are known. A typical hydraulic circuit used for servo-positioning systems (figure 4.1) can be analyzed as two distinct subsystems: a servo-actuator system and a hydraulic supply system. The hydraulic supply consists of a pressure compensating variable displacement pump supplying compliant hydraulic lines. The servo-actuator system consists of a two-stage servovalve connected to a hydraulic actuator which in turn moves the ram. In the following sections, the physics of the servo-actuator system is
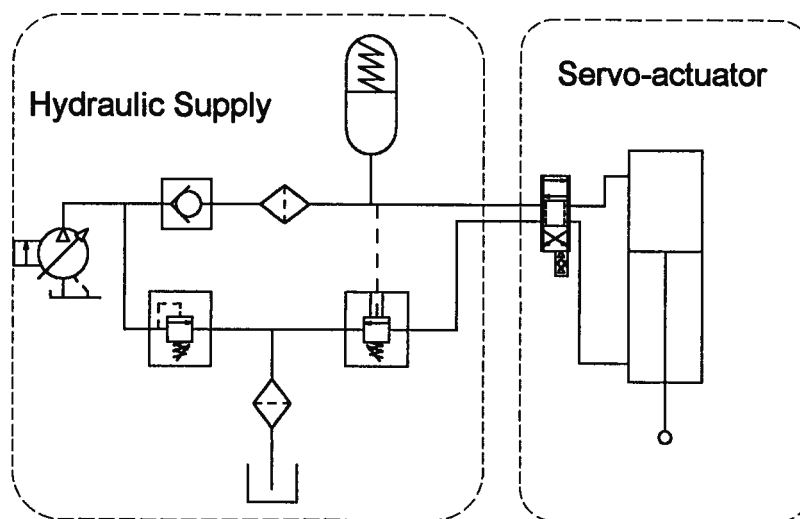
Figure 4.1. Typical hydraulic system used for servo positioning.

described and models used to represent the dynamics are presented.

## 4.2 Dynamic Model of Servo-actuator

The servo-actuator used to position each joint of the ram can be considered as a system consisting of three distinct subsystems:a precision flow-control valve, a hydraulic cylinder and a load (figure 4.1).
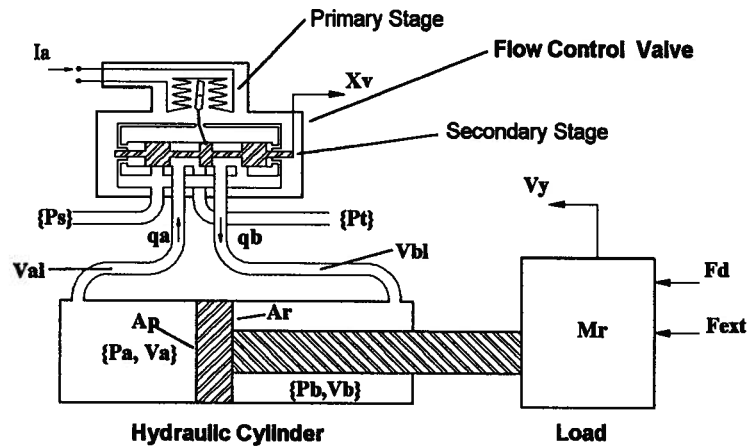


Figure 4.2. Functional diagram of servo-actuator.

The flow control valve used for the positioning system is a two-stage servovalve. The primary stage consists of an electronic torque motor driving a primary valve, usually of a flapper or a jet-pipe type (flapper-valve type shown in figure 4.2). When the torque-motor is driven, the primary valve provides a differential pressure across the ends of a secondary closed-centre spool valve. The displacement of the secondary spool is fed back to the torque motor by way of a cantilever spring. This spool controls the flow to the cylinder. The position of the flow controlling spool as a function of the torque motor current can be represented by a first-order lag due to the torque motor combined with a quadratic lag due to the dynamics of the spool:

$$\frac{x_v(s)}{i_a(s)} = \frac{K_i}{(\tau_i s + 1)(s^2 + 2\zeta_v \omega_v s + \omega_v{}^2)},$$ (4.1)

where:

$x_v$: spool displacement

$i_a$: torque motor current

$K_i$: spool valve positioning gain

$\omega_v$: natural frequency of spool dynamics

$\zeta_v$: coefficient of friction for spool valve

Generally, the dynamics of the spool are considerbly faster than the dynamics of the torque motor so that (4.1) can be approximated by the following expression:

$$\frac{x_v(s)}{i_a(s)} \cong \frac{K_i'}{(\tau_i s + 1)},$$ (4.2)

where:

$K_i'$: effective spool valve positioning gain

The flow through a port of the secondary-stage spool valve has been found to be proportional to the area of the valve opening and the square root of the pressure drop across the port. Since the area of the valve opening is proportional to the valve displacement, the following expressions can be used to represent the flow through the ports of a spool valve:

for $x_v \geq 0$,

$$q_a = K_{qa} x_v \sqrt{|P_s - p_a|} \, sign(P_s - p_a)$$ (4.3)

$$q_b = K_{qb} x_v \sqrt{|p_b - p_t|} \, sign(p_b - p_t)$$ (4.4)

for $x_v < 0$,

$$q_a = K_{qa} x_v \sqrt{|p_a - p_t|} \, sign(p_a - p_t)$$ (4.5)

$$q_b = K_{qb} x_v \sqrt{|p_s - p_b|} \, sign(p_s - p_b)$$ (4.6)

where:

$q_a$: flow out of port A of valve

$q_b$: flow into port B of valve

$K_{qa}, K_{qb}$: coefficients of flow for ports A and B

$p_s$: supply line pressure

$p_t$: return line (tank) pressure

$p_a, p_b$: pressure acting upon ports A and B of the valve

The hydraulic cylinder, as depicted in figure 4.2 consists of two fluid chambers separated by a piston. The rod connecting the piston to the rod is assumed to be rigid. Because the fluid on either side of the piston is mildly compressible, hydraulic cylinders exhibit compliance under load. This compliance (or its inverse, stiffness) is a concern to servo-system designers because it limits the maximum bandwidth of the system.

To determine a relationship between the chamber pressures, chamber flows and piston velocity, the continuity equation can be applied to control volumes encompassing each chamber to obtain the following expressions:

$$q_a - q_{c_a} - K_{lp}(p_a - p_b) = -A_p v_y \qquad (4.7)$$

$$q_b + q_{c_b} + K_{lp}(p_b - p_a) + K_{le}p_b = -A_r v_y \qquad (4.8)$$

where:

$v_y$: velocity of the piston

$A_p$: area of the piston

$A_r$: area of the piston minus the area of the rod

$K_{lp}$: coefficient of leakage past the piston

$K_{le}$: coefficient of leakage past the rod seals

$q_{c_a}$: rate of change of volume due to volume A compliance

$q_{c_b}$: rate of change of volume due to volume B compliance

Since fluid compressibility is directly proportional to the volume in which the pressure acts, the compliance of each actuator chamber may be expressed as:

$$C_a = \frac{1}{\beta_e}(V_{al} + A_p(L-y)),$$ (4.9)

$$C_b = \frac{1}{\beta_e}(V_{bl} + A_r y),$$ (4.10)

where:

$V_{a_l}, V_{b_l}$: volume of fluid in the line leading to chambers A and B

$\beta_e$: bulk modulus of the fluid

$y$: piston position

If the fluid compliance relations, (4.9) and (4.10), are linearized about a particular operating point $(L_0)$, the following expressions for the rate of change of volume within the actuator may be written:

$$q_{ca} = \overline{C}_a \frac{dp_a}{dt}$$ (4.11)

$$q_{cb} = \overline{C}_b \frac{dp_b}{dt}$$ (4.12)

where:

$\overline{C}_a$: linearized compliance of fluid in chamber A

$\overline{C}_b$: linearized compliance of fluid in chamber B

By summing the forces acting on the load mass, the following equation for the motion of the load can be written:

$$\sum F_{\leftarrow}^+ = M_r \frac{dv_y}{dt} = A_r p_b - A_p p_a - B_r v_y - F_c sign(v_y) + F_{ext}$$ (4.13)

where:

$M_r$: combined effective mass of piston and load

$B_r$: effective viscous damping actuator

$F_c$: coulomb friction force

$F_{ext}$: external load (including gravity)

Equations (4.1-4.13) are the fundamental epressions most models use to study cylindrical hydraulic servo-actuators.

## 4.2.1 The Load Pressure, Load Flow Model

Most of the research concerning cylindrical hydraulic servo-actuators pertains to the case where there is equal area on each side of the piston: i.e. symmetric actuators. Although most hydraulic presses do not employ such actuators, an analysis of such models is worthwhile because they provide the simplest estimation of system performance. Merritt [14] presents a thorough analysis of symmetric hydraulic actuators utilizing a simple linear model based on a load pressure, load flow (LPLF) simplification.

In order to reduce (4.1-4.13) to a linear model numerous assumptions need to be made. By assuming zero tank pressure, no cavitation and a symmetric actuator, the flows into and out of the spool valve can be equated so that the following expression, normalized with respect to the supply pressure, holds:

$$q_l = K_q x_v \sqrt{1 - \frac{p_l}{p_s}}, \tag{4.14}$$

where:

$q_l$: effective load flow $(q_a - q_b)$

$K_q$: normalized valve flow gain

$p_l$: effective load pressure $(p_a - p_b)$

If the spool only undergoes small disturbances about the null flow position, (4.14) can be linearized to yield:

$$q_l = K_q x_v - K_c p_l, \tag{4.15}$$

where:

$K_c$: null flow pressure gain

Since this linearization yields a zero value for the null flow pressure coefficient, this value is usually determined empirically from closed-port leakage tests [14].

To extend this LPLF analysis to the actuator, the load is assumed to undergo relatively small excursions from a set operating point. Furthermore, if it is assumed the

fluid in each chamber is of equal compliance, (4.7-4.10) can be linearized and combined to yield:

$$q_l = -A_p v_y + K_l p_l + C_{ab} \frac{dp_l}{dt}, \qquad (4.16)$$

where:

$$K_l = K_{li} + \frac{K_{le}}{2}$$

$$C_{ab} = \frac{V_t}{4\beta_e}$$

$V_t$: total volume of fluid within the cylinder and lines

Equation (4.16) can be combined with (4.15) and rearranged to yield, using Laplace notation:

$$p_l = \frac{K_q x_v + A_p v_y}{C_{ab} s + K_{ctm}}, \qquad (4.17)$$

where:

$$K_{ctm} = K_l + K_c. \qquad (4.18)$$

Considering the equation defining the load dynamics (4.13), some assumptions must be made to accommodate the coulomb damping term. In the past coulomb damping has been modeled with viscous damping [21,23], but modern analysis considers coulomb friction to be an external disturbance. If the damping is assumed to be strictly viscous, the load equation (4.13) can be rewritten, using Laplace notation:

$$M_r s v_y + B_r v_y = -A_p p_l + F_{ext} \qquad (4.19)$$

Combining (4.17) and (4.19) yields the following transfer functions for the response of the servoactuator to the spool displacement and the external force:

$$\frac{v_y(s)}{x_v(s)} = \frac{K_x}{s^2 + 2\zeta_l \omega_l s + \omega_l^2}, \qquad (4.20)$$

$$\frac{v_y(s)}{F_{ext}(s)} = \frac{K_{Fext}(\tau_{ab}s+1)}{s^2 + 2\zeta_l\omega_l s + \omega_l^2} \tag{4.21}$$

where:

$$\zeta_l = \frac{K_{ctm}}{A_p}\sqrt{\frac{\beta_e M_r}{V_t}} + \frac{B_r}{4A_p}\sqrt{\frac{V_t}{\beta_e M_r}} \tag{4.22}$$

$$\omega_l = \sqrt{\frac{4\beta_e A_p^2}{V_t M_r}\left(1 + \frac{K_{ctm}B_r}{A_p^2}\right)} \tag{4.23}$$

$$K_x = \frac{4\beta_e A_p K_q}{V_t M_r} \tag{4.24}$$

$$\tau_{ab} = \frac{V_t}{4K_{ctm}\beta_e} \tag{4.25}$$

$$K_{Fext} = \frac{1}{\tau_{ab}M_r} \tag{4.26}$$

It has been noted that the contribution of viscous damping in this type of drive is very small [9,17,19]. Hence, it is common practice to assume $B_r = 0$. Using this assumption, (4.22) and (4.23) reduce to:

$$\zeta_l = \frac{K_{ctm}}{A_p}\sqrt{\frac{\beta_e M_r}{V_t}}, \text{ and} \tag{4.27}$$

$$\omega_l = \sqrt{\frac{4\beta_e A_p^2}{V_t M_r}}, \tag{4.28}$$

which indicates two phenomena characteristic of all valve-controlled actuators. First, for a cylinder with minimal external leakage, the damping is proportional to the cross port leakage (null position valve leakage and piston leakage). Second, the stiffness of the actuator is proportional to the bulk modulus of the fluid and the piston area while being inversely proportional to the stroke. Because of their inherent simplicity, (4.27) and (4.28) are often used during the preliminary stages of servoactuator design [28]. Intuitive

variations of (4.27) and (4.28) exist for the design of servoactuators utilizing non-symmetrical hydraulic cylinders.

The chief virtue of the LPLF model is its conservative estimate of system performance. Since the derivation makes use of a control valve linearization about the operating point with the least damping (the null position), the LPLF model gives a lower bound for damping within the system. Furthermore, since the actuator compliance expressions relations (4.9) and (4.10) are linearized about the most compliant piston position, this model also provides a lower bound for the bandwidth of the system.

## 4.2.2 Improved Frequency Response Model

While the LPLF model can be used to determine the frequency response of a servoactuator system, McCloy and Martin [13] present a more sophisticated model which considers the effect of the spool valve displacement on the damping of the system. This improved frequency response (IFR) model is based upon the LPLF model.

Assuming a pure inertia load, (i.e., no damping and no external load), and a symmetric actuator (piston area $A_p$) the expression describing the load dynamics (4.13) can be simplified to:

$$M_r \frac{dv_y}{dt} = A_p(p_b - p_a),$$
(4.29)

or,

$$p_l = -\frac{M_r}{A_p}\frac{dv_y}{dt}.$$
(4.30)

Rewriting the non-linear pressure/flow relationship for the LPLF model (4.14) in non-normalized form yields:

$$q_l = K_q' x_v \sqrt{P_s - p_l}.$$
(4.31)

$$K'_q = \frac{K_q}{\sqrt{P_s}}$$

Substituting (4.30) into (4.31) yields:

$$q_l = K'_q x_v \sqrt{P_s + \frac{M_r}{A_p}\frac{dv_y}{dt}} \, . \tag{4.32}$$

If 4.32 is linearized about the point of maximum load velocity, ($\frac{dv_y}{dt} = 0$), the following

expression for the load flow is obtained:

$$q_l = K'_q x_v \sqrt{P_s}(1 + \frac{1}{2}\frac{M_r}{A_p P_s}\frac{dv_y}{dt}) \tag{4.33}$$

or the more general form:

$$q_l = K_q x_v (1 + \lambda \frac{M_r}{A_p P_s}\frac{dv_y}{dt}), \tag{4.34}$$

where:

$\lambda$: flow/pressure linearization constant

McCloy and Martin [13] suggest using a value of $\lambda$ in (4.34) other than 1/2. The criterion used to select $\lambda$ is minimum error between the actual pressure/flow relation and the linearized relation (4.34). This criterion yields a value of 2/3.

Assuming no actuator leakage ($K_l = 0$), (4.34) can be combined with (4.16) to produce:

$$K_q x_v (1 + \lambda \frac{M_r}{A_p P_s}\frac{dv_y}{dt}) = -A_p v_y - \frac{V_t M_r}{4\beta_e A_p}\frac{d^2 v_y}{dt^2} \tag{4.35}$$

or, by rearranging:

$$\frac{d^2 v_y}{dt^2} + \frac{dv_y}{dt}(4\lambda\frac{K_q x_v \beta_e}{V_t P_s}) + v_y(4\frac{\beta_e A_p^2}{V_t M_r}) = -K_q x_v(4\frac{\beta_e A_p}{V_t M_r}). \tag{4.36}$$

For a harmonic input with a fixed amplitude of the form:

$$x_v(t) = X_v \sin(\omega t),$$
(4.37)

the frequency response can be expressed by the relation:

$$\frac{v_y(j\omega)}{x_v(j\omega)} = \frac{K_x}{\omega_l^2 - \omega^2 + 2j\zeta_l(X_v)\omega_l\omega},$$
(4.38)

where:

$$\zeta_l(X_v) = \lambda \frac{K_q X_v}{p_s A_p} \sqrt{\frac{\beta_e M_r}{V_t}},$$
(4.39)

and, as in the LPLF model (4.27 and 4.28):

$$\omega_l = \sqrt{\frac{4\beta_e A_p^2}{V_t M_r}}, \quad \text{and} \quad K_x = \frac{4\beta_e A_p K_q}{V_t M_r}.$$
(4.40)

In order to produce a harmonic spool motion, a harmonic current signal of the form:

$$i_a(t) = I_a \sin(\omega t),$$
(4.41)

has to be applied to the torque motor of the servo valve. When the dynamics of the primary stage of the servovalve are included (4.2), an expression for the frequency response of the load velocity with respect to the servovalve input signal can be written:

$$\frac{v_y(j\omega)}{i_a(j\omega)} = \frac{K_i' K_x}{\omega_l^2 - \omega^2 - 2\tau_i\omega_l\omega^2\zeta_l'(I_a) + j(\tau_i\omega\omega_l^2 - \tau_i\omega^3 + 2\omega_l\omega\zeta_l'(I_a))}$$
(4.42)

where:

$$\zeta_l'(I_a) = \lambda \frac{K_q K_i' I_a}{p_s A_p} \sqrt{\frac{\beta_e M_r}{V_t}},$$
(4.43)

From (4.42) and (4.43) it is evident the IFR model can be used to determine the frequency response for a particular amplitude of excitation. However, as with the LPLF model, the IFR model assumes symmetrical actuators. If the ratio of the cap-side to rod-side piston area ($R$) is not unity, a more appropriate model may be required.

## 4.2.3 A Directionally Biased Model for Asymmetrical Actuators

Although many investigations of the dynamics characteristics of servosystems employing non-symmetrical actuators have been conducted, most either ignore the effects of fluid compressibility[24] or assume equal fluid chamber compliance. An exception to this trend is presented by Watton [29]. In this study, the stability and step response of a proportionally-controlled, symmetrical servoactuator are studied for cases where the ratio of the volume of oil on each side of the piston is not unity. An application of the analysis used in this investigation follows.

Given the pressure/flow relations (4.3-4.6), linearized relations for the flow through each port of the spool can be written:

for $x_v \geq 0$,

$$q_a = {}^+K_{qa}x_v - {}^+K_{ca}P_a \tag{4.44}$$

$$q_b = {}^+K_{qb}x_v + {}^+K_{cb}P_b \tag{4.45}$$

for $x_v < 0$,

$$q_a = {}^-K_{qa}x_v - {}^-K_{ca}P_a \tag{4.46}$$

$$q_b = {}^-K_{qb}x_v + {}^-K_{cb}P_b \tag{4.47}$$

where:

$\quad {}^+K_{qa}, {}^+K_{qb}$: A & B port flow gains when $x_v \geq 0$

$\quad {}^-K_{qa}, {}^-K_{qb}$ A & B port flow gains when $x_v < 0$

$\quad {}^+K_{ca}, {}^+K_{cb}$: A & B port pressure coefficients when $x_v \geq 0$

$\quad {}^-K_{ca}, {}^-K_{cb}$: A & B port pressure coefficients when $x_v < 0$

or, more generally,

$$q_a = {}^dK_{qa}x_v - {}^dK_{ca}P_a \tag{4.48}$$

$$q_b = {}^dK_{qb}x_v + {}^dK_{cb}P_b \tag{4.49}$$

where:

$$d \;:\; \text{'+' when } x_v \geq 0$$

$$d : \text{'-' when } x_v < 0$$

If the actuator flow expressions, (4.46-4.49), are linearized about a particular piston position, and external leakage is neglected, the following expressions can be written:

$$q_a = -A_p v_y + K_{lp}(p_a - p_b) + C_a \frac{dp_a}{dt} \tag{4.50}$$

$$q_b = -A_r v_y + K_{lp}(p_a - p_b) - C_b \frac{dp_b}{dt} \tag{4.51}$$

Combining (4.48-4.49) with (4.50-4.51) yields:

$${}^d K_{qa} x_v - {}^d K_{ca} p_a = -A_p v_y + K_{lp}(p_a - p_b) + C_a \frac{dp_a}{dt} \tag{4.52}$$

$${}^d K_{qb} x_v + {}^d K_{cb} p_b = -A_r v_y + K_{lp}(p_a - p_b) - C_b \frac{dp_b}{dt}, \tag{4.53}$$

These expressions can be rewritten using Laplace notation:

$$p_a = \frac{{}^d K_{qa} x_v + A_p v_y + K_{lp} p_b}{C_a s + ({}^d K_{ca} + K_{lp})} \tag{4.54}$$

$$p_b = -\frac{{}^d K_{qb} x_v + A_p v_y - K_{lp} p_a}{C_b s + ({}^d K_{cb} + K_{lp})} \tag{4.55}$$

Considering (4.13), the following expression describing the dynamics of the load can be written using Laplace notation:

$$M_r v_y s + B_r v_y = A_r p_b - A_p p_a + F_{ext} \tag{4.56}$$

Combining (4.54-4.56) yields the following transfer functions:

$$\frac{v_y(s)}{x_v(s)} = -\frac{{}^d K_{xv}(\tau_{xv} s + 1)}{s^3 + a_1 s^2 + a_2 s + a_3} \tag{4.57}$$

$$\frac{v_y(s)}{F_{ext}(s)} = \frac{1}{M_r} \frac{s^2 + b_1 s + b_2}{s^3 + a_1 s^2 + a_2 s + a_3} \tag{4.58}$$

where:

$$a_1 = \frac{B_r}{M_r} + \frac{K_a}{C_a} + \frac{K_b}{C_b}$$

$$a_2 = \frac{\left(K_a K_b - K_{lp}^{2}\right)}{C_a C_b} + \left(\frac{K_a}{C_a} + \frac{K_b}{C_b}\right)\frac{B_r}{M_r} + \left(\frac{A_p^{2}}{C_a} + \frac{A_r^{2}}{C_b}\right)\frac{1}{M_r}$$

$$a_3 = \frac{\left(K_a K_b - K_{lp}^{2}\right)B_r + A_r^{2} K_a + A_p^{2} K_b - 2 A_r A_p K_{lp}}{C_a C_b M_r}$$

$$b_1 = \frac{K_a}{C_a} + \frac{K_b}{C_b} \qquad\qquad b_2 = \frac{K_a K_b - K_{lp}^{2}}{C_a C_b}$$

$${}^d K_{xv} = \frac{A_r\left(K_a K_{qb} - K_{lp} K_{qa}\right) + A_p\left(K_b K_{qa} - K_{lp} K_{qb}\right)}{C_a C_b M_r}$$

$$\tau_{xv} = \frac{A_r K_{qb} C_a + A_p K_{qa} C_b}{A_r\left(K_a K_{qb} - K_{lp} K_{qa}\right) + A_p\left(K_b K_{qa} - K_{lp} K_{qb}\right)}$$

$$K_a = {}^d K_{ca} + K_{lp} \qquad\qquad K_b = {}^d K_{cb} + K_{lp}$$

It has been shown that (4.57) and (4.58) reduce to the LPLF expressions (4.20) and (4.21) respectively, when the piston area ratio is unity and the actuator volume compliances, $C_a$ and $C_b$ are equal [29].

## 4.2.4 Non-Linear Valve Flow Relation

The models presented so far, which have commonly been used to design hydraulic servo actuator systems, all assume a linearized flow/pressure relationship. Although it has been concluded that this assumption is valid for a significant range of load pressures and valve openings, the accurate prediction of the large signal response of a hydraulic servo requires the non-linear flow/pressure characteristics of the secondary spool valve to be considered. To this end, several non-linear models have been developed. The following is

a description of a particular model used to numerically simulate the response of the servoactuator system.

From the manufacturer's information, the response of the spool of the valve to an armature current can be represented by a first order lag, such that:

$$\frac{x_v(s)}{i_a(s)} = \frac{K_i}{\tau_v s + 1}, \tag{4.59}$$

Combining expressions (4.3-4.8) and solving for the rate of change of volume due to fluid compressibility (or the compliance flows):

for $x_v \geq 0$,

$$q_{ca} = K_{qa} x_v \sqrt{|P_s - p_a|} sign(p_s - p_a) + A_p v_y - K_{lp}(p_a - p_b), \tag{4.60}$$

$$q_{cb} = -K_{qb} x_v \sqrt{|p_b - p_t|} sign(p_b - p_t) - A_r v_y - K_{lp}(p_b - p_a) - K_{le} p_b \tag{4.61}$$

for $x_v < 0$,

$$q_{ca} = K_{qa} x_v \sqrt{|p_a - p_t|} sign(p_a - p_t) + A_p v_y - K_{lp}(p_a - p_b), \tag{4.62}$$

$$q_{cb} = -K_{qb} x_v \sqrt{|P_s - p_b|} sign(p_s - p_b) - A_r v_y - K_{lp}(p_b - p_a) - K_{le} p_b \tag{4.63}$$

## 4.2.5 Non-Linear Actuator Compliance

It has been shown that the change of actuator compliance with piston position has only a minor effect on the response of symmetrical actuators [11]. However, for asymmetrical actuators, the relative change of compliance for a change in piston position is magnified by the ratio of the area on each side of the piston. To investigate this phenomena, two alternative models were developed: one based on a flow causal relation, the other base on a pressure causal relation.

The derivation of the flow causal compliance (FCC) model is based upon the following assertion: the pressure increase in a control volume is equal to the integral of the flow entering the volume divided by the compliance of the fluid in the volume. For control volume A this assertion is represented by the following expression:

$$p_a(t) = \int \frac{1}{C_a(t)} q_{ca}(t)dt \tag{4.64}$$

Since the compliance of the control volume (4.9) is a function of the piston position, (4.64) can be rewritten:

$$p_a(t) = \beta_e \int \frac{q_{ca}(t)}{\left(V_{al} + A_p(L - y(t))\right)} dt \tag{4.65}$$

Differentiating (4.65) and solving for the compliance flow yields (dropping the time function notation):

$$q_{ca} = \frac{dp_a}{dt} \frac{1}{\beta_e} \left(V_{al} + A_p(L - y)\right). \tag{4.66}$$

A similar expression can be derived for control volume B:

$$q_{cb} = \frac{dp_b}{dt} \frac{1}{\beta_e} \left(V_{bl} + A_r y\right). \tag{4.67}$$

Substituting (4.66) and (4.67) into (4.62) and (4.63) and solving for $\frac{dp_a}{dt}$ and $\frac{dp_b}{dt}$ yields the following control volume pressure relations for the FCC model:

for $x_v \geq 0$,

$$\frac{dp_a}{dt} = \beta_e \frac{K_{qa} x_v \sqrt{|p_s - p_a|} sign(p_s - p_a) - K_{lp}(p_a - p_b) + A_p v_y}{V_{al} + A_p(L - y)} \tag{4.68}$$

$$\frac{dp_b}{dt} = -\beta_e \frac{K_{qb} x_v \sqrt{|p_b - p_t|} sign(p_b - p_t) + K_{lp}(p_b - p_a) + K_{le} p_b + A_r v_y}{V_{bl} + A_r y} \tag{4.69}$$

for $x_v < 0$,

$$\frac{dp_a}{dt} = \beta_e \frac{K_{qa} x_v \sqrt{|p_a - p_t|} sign(p_a - p_t) - K_{lp}(p_a - p_b) + A_p v_y}{V_{al} + A_p(L - y)} \tag{4.70}$$

$$\frac{dp_b}{dt} = -\beta_e \frac{K_{qb} x_v \sqrt{|p_s - p_b|} sign(p_s - p_b) + K_{lp}(p_b - p_a) + K_{le} p_b + A_r v_y}{V_{bl} + A_r y} \tag{4.71}$$

The derivation of the pressure causal compliance (PCC) model is based upon a somewhat different assertion: the rate of change of the volume of fluid compressed (the compliance flow) is proportional to the rate of change of the product of the compliance and the pressure. For control volume A this can be written as:

$$q_{ca}(t) = \frac{d}{dt}\big(C_a(t)p_a(t)\big) \tag{4.72}$$

Substituting (4.9) for $C_a(t)$, (4.72) can be rewritten:

$$q_{ca}(t) = \frac{d}{dt}\left(\frac{1}{\beta_e}\big(V_{al} + A_p(L - y(t))\big)p_a(t)\right) \tag{4.73}$$

Differentiating the expression in parenthesis of (4.73) yields (dropping the time function notation):

$$q_{ca} = \frac{dp_a}{dt}\frac{\big(V_{al} + A_p(L - y)\big)}{\beta_e} - p_a \frac{A_p}{\beta_e}v_y \tag{4.74}$$

For control volume B, this analysis yields:

$$q_{cb} = \frac{dp_b}{dt}\frac{\big(V_{bl} + A_r y\big)}{\beta_e} + p_b \frac{A_r}{\beta_e}v_y \tag{4.75}$$

For the PCC model, substituting (4.74) and (4.75) into (4.62) and (4.63) and solving for $\frac{dp_a}{dt}$ and $\frac{dp_b}{dt}$ yields the following actuator control volume pressure relations:

for $x_v \geq 0$,

$$\frac{dp_a}{dt} = \beta_e \frac{K_{qa}\, x_v \sqrt{|p_s - p_a|}\,sign(p_s - p_a) - K_{lp}(p_a - p_b) + A_p v_y\left(1 + \frac{p_a}{\beta_e}\right)}{V_{al} + A_p(L - y)} \tag{4.76}$$

$$\frac{dp_b}{dt} = -\beta_e \frac{K_{qb}\, x_v \sqrt{|p_b - p_t|}\,sign(p_b - p_t) + K_{lp}(p_b - p_a) + K_{le}p_b + A_r v_y\left(1 + \frac{p_b}{\beta_e}\right)}{V_{bl} + A_r y} \tag{4.77}$$

for $x_v < 0$,

$$\frac{dp_a}{dt} = \beta_e \frac{K_{qa} x_v \sqrt{|p_a - p_t|} sign(p_a - p_t) - K_{lp}(p_a - p_b) + A_p v_y \left(1 + \frac{p_a}{\beta_e}\right)}{V_{al} + A_p(L - y)} \tag{4.78}$$

$$\frac{dp_b}{dt} = -\beta_e \frac{K_{qb} x_v \sqrt{|p_s - p_b|} sign(p_s - p_b) + K_{lp}(p_b - p_a) + K_{le}p_b + A_r v_y \left(1 + \frac{p_b}{\beta_e}\right)}{V_{bl} + A_r y} \tag{4.79}$$

Since, for all practical purposes, $\frac{p_a}{\beta_e} << 1$ and $\frac{p_b}{\beta_e} << 1$ expressions (4.76-4.79) can be

simplified to the expressions derived using the FCC model (4.68-4.71).

While the load relation (4.13) is valid while the piston is moving, it is desirable to

augment this expression so as to ensure mathematical validity when the velocity of the

piston is zero. The following expression can be used:

$$\sum F^+_{\leftarrow} = M_r \frac{dv_y}{dt} = A_r p_b - A_p p_a - B_r v_y - F_{cd} + F_{ext} \tag{4.80}$$

where:

for:     $\left| A_r p_b - A_p p_a + F_{ext} \right| < F_c$:

$$F_{cd} = A_r p_b - A_p p_a + F_{ext}$$

and for:     $\left| A_r p_b - A_p p_a + F_{ext} \right| \geq F_c$

$$F_{cd} = F_c sign(v_y)$$

$$\tag{4.81}$$

These equations (4.59-4.63, 4.68-4.71, 4.80-4.81) can be arranged as a series of non-

linear state equations which can be solved numerically to determine the system response to

a series of inputs.

The values of the system model parameters are presented in Appendix D.

## 4.3 Results

### 4.3.1 The Effect of the LPLF Linearization on the System Response

A comparison between the step response predicted by the LPLF model and the response predicted by the non-linear LC model for a symmetric actuator with no external load is shown in figure 4.3. For the valve opening step, (0 < t < 125ms) the response
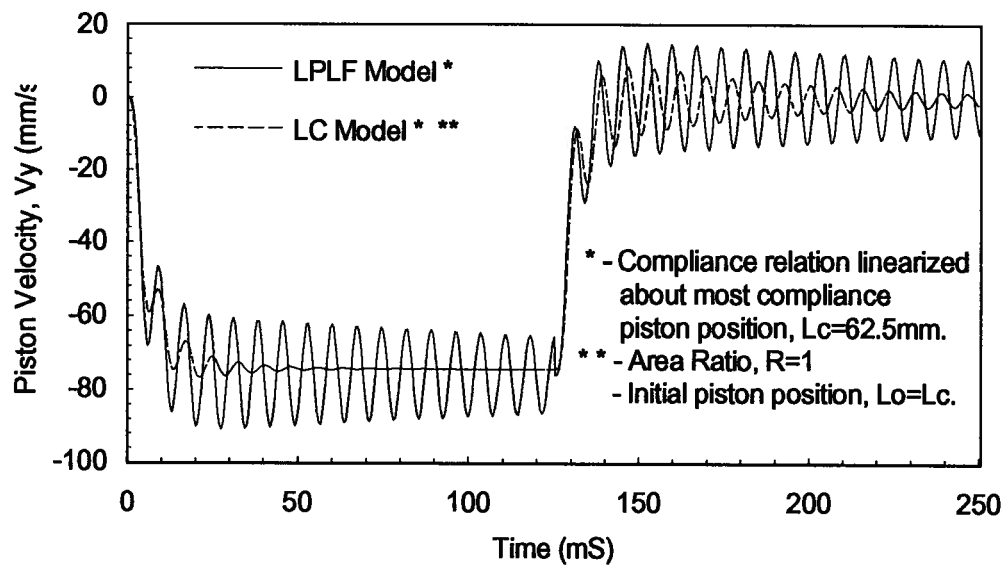


Figure 4.3. Comparison of velocity response predicted by LPLF model versus the velocity predicted by the LC model with piston area ratio R=1.

predicted by the LPLF model is significantly more oscillatory than that predicted by the LC model. This can be attributed to the fact that the LPLF model is based upon a linearization about the valve null position, the position exhibiting the least damping. For the valve closing step (125 < t < 250ms) both models predict an oscillatory response, with the LC model exhibiting greater damping. Also, from this plot, the capability of the LPLF model to predict the steady-state velocity of a symmetrical actuator is exhibited.

## 4.3.2 The Effect of Piston Area Ratio the System Response

A comparison of the velocity response of two actuator system: one with a symmetric actuator, the other with an asymmetric actuator is shown in 4.4. While the response of the two systems is similar, the steady state velocities are different and the systems oscillate at slightly different frequencies.

## 4.3.3 The Effect of Input Signal Amplitude on the System Response

In order to examine the effect of the amplitude of the servovalve command signal on the response of the system, the frequency response predicted by the LPLF model was compared to the frequency response predicted by the IFR model for various values of input armature current. The results are presented in figure 4.5. From this plot, it is evident that the system response exhibits much greater damping as the amplitude of the
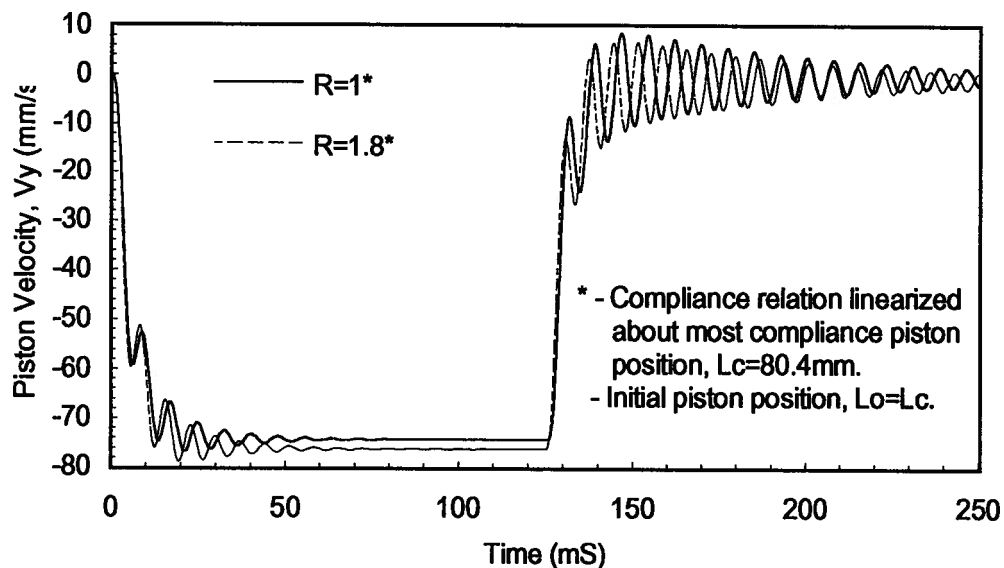
Figure 4.4. Comparison of the effect of piston area ratio, R, on the velocity response of servoactuator, as predicted by the LC model.

input signal is increased. Also, as the amplitude of the input signal approaches zero the frequency response predicted by the IFR model approaches that predicted by the LPLF model. This phenomena can be explained by the fact that the LPLF model's damping term is linearized about the null flow position which is approached as the amplitude of the input signal is reduced. The system bandwidth (-3 dB) is approximately 30 Hz.
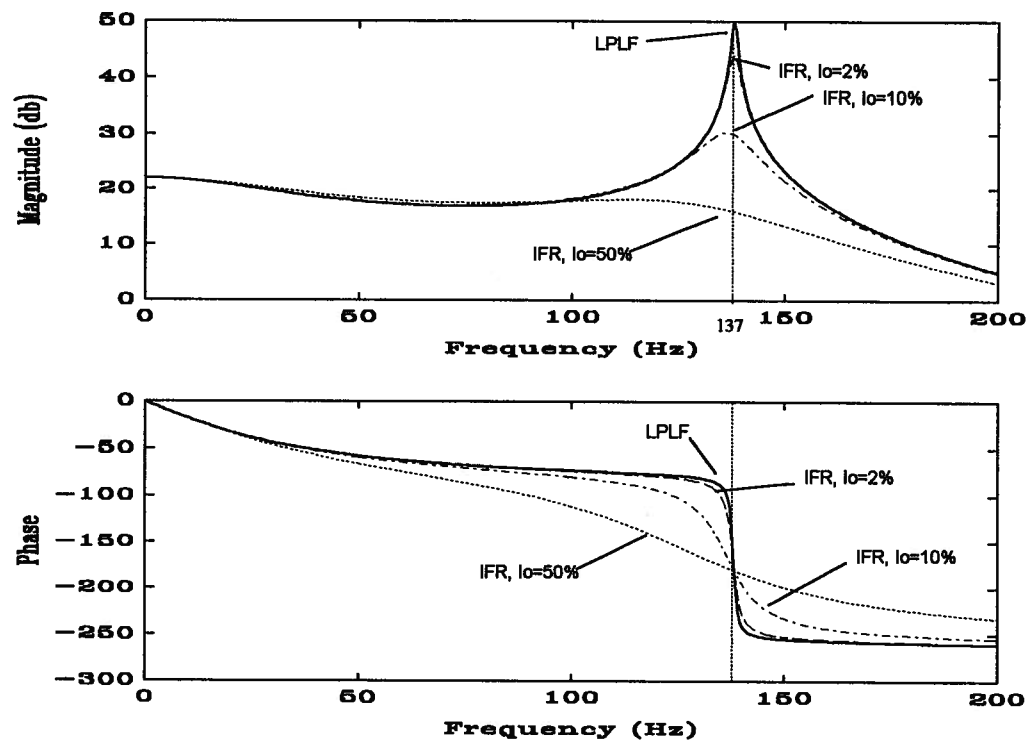


Figure 4.5. Comparison of the frequency response predicted by the LPLF model to that predicted by the IFR model at various servovalve armature current amplitudes.

## 4.3.4  The Effect of Initial Piston Position on the System Response

In this section, a comparison of step response predicted by the non-linear servo-actuator model utilizing a linearized compliance relation (LC Model) and that predicted by the non-linear model utilizing the flow-causal compliance relation (FCC Model) is examined. For this comparison, the compliance relation of the LC model is linearized about the critical piston position (i.e., the position yielding the maximum actuator compliance). In the first comparison, figure 4.6, the response predicted by the LC model is compared to the response predicted by the FCC model when the initial position is the critical position. In this case, the models compare quite favorably. In the second comparison, figure 4.7, the initial position of the actuator is varied from one limit to the other. In this case the FCC model predicts a much better damped response than the LC model. These plots indicate two things: i) the systems response tends to be less oscillatory
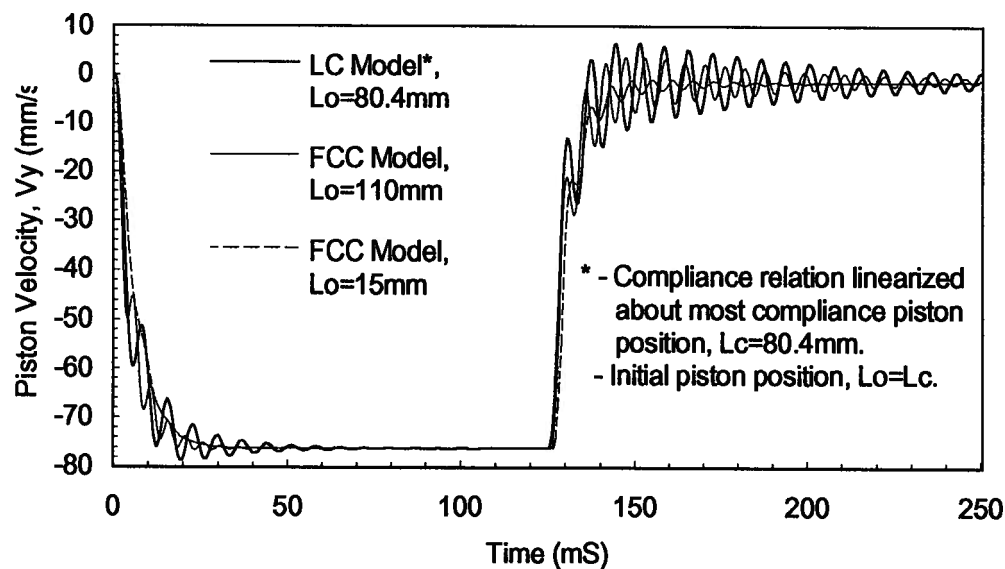


Figure 4.6. Comparison of the Velocity response predicted by LC model versus that predicted by the FCC model when the initial position differs from the LC linearization position.

away from the most compliant position, ii) the LC model should be linearized about a

piston position in which the actuator will operate. However, if the higher order dynamics

of the actuator become significant, the LC model will not provide an accurate description

of the system dynamics away from the linearization point.
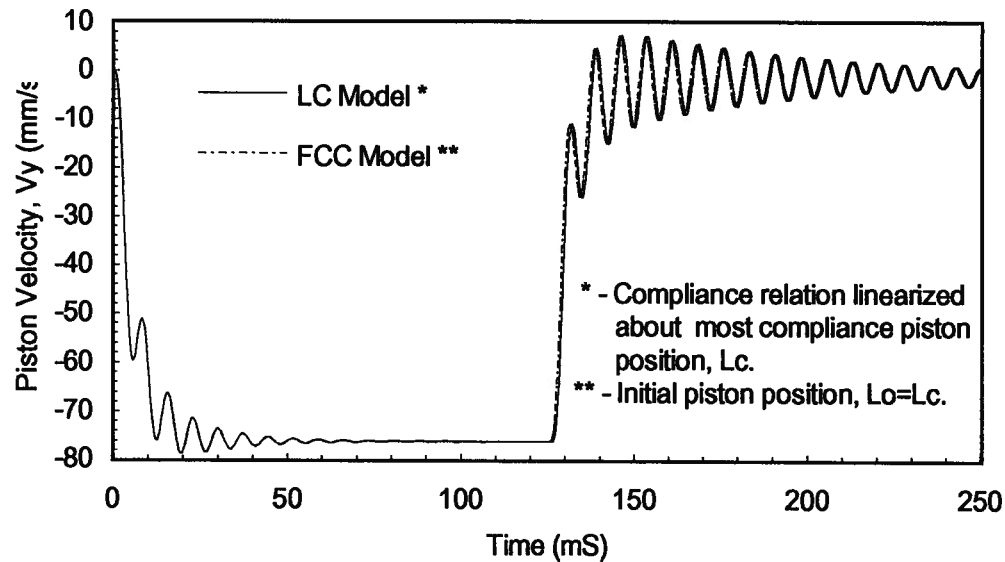


Figure 4.7. Comparison of the response predicted by LC model versus that predicted by
the FCC model when the initial position corresponds to the LC linearization position.

## 4.3.5 Effect of Coulomb Friction on the System Response

The positioning system has been found to have significant non-linear friction

characteristics (see Appendix C). The dominant non-linear characteristics can be modeled

by coulomb friction. In order to investigate the effect of this type of friction on the system

response characteristics, the system was simulated using the LC model for various

amounts of coulomb friction (figure 4.8). From this plot we can observe that the quantity

of coulomb friction in the system has a negligible effect on the steady-state velocity of the

system while the control spool is open, but contributes substantially to the damping of the system when the control spool is closed.

Since the valve-closing condition is the most critical in terms of position control, this friction may lend a stabilizing effect to the overall system dynamics.
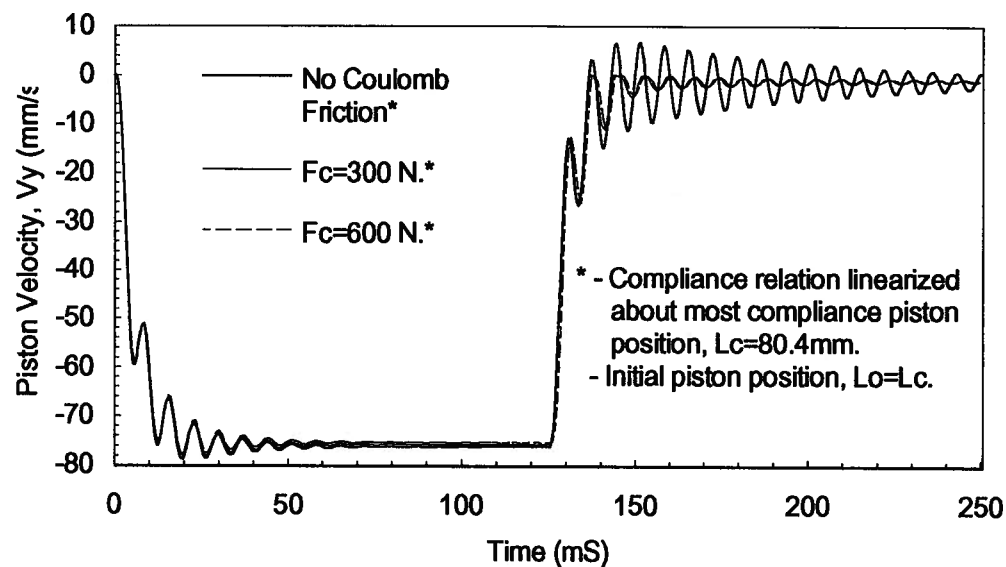


Figure 4.8. Comparison of the effect of coulomb friction, Fc, on the velocity response of the system as predicted by the LC model.

## 4.3.6 Validation of the Non-Linear Models

A comparison between the measured response of the servoactuator system to a multi-step input and the response predicted by the LC and FCC models is presented in figure 4.9. From this plot we can observe that the LC and FCC models match the trend of the actual system reasonably well. However, the actual system response does not exhibit an oscillating response as predicted by the two models. This discrepancy can be attributed

to unmodeled leakage across the piston seals which was not readily obtainable using the equipment available.
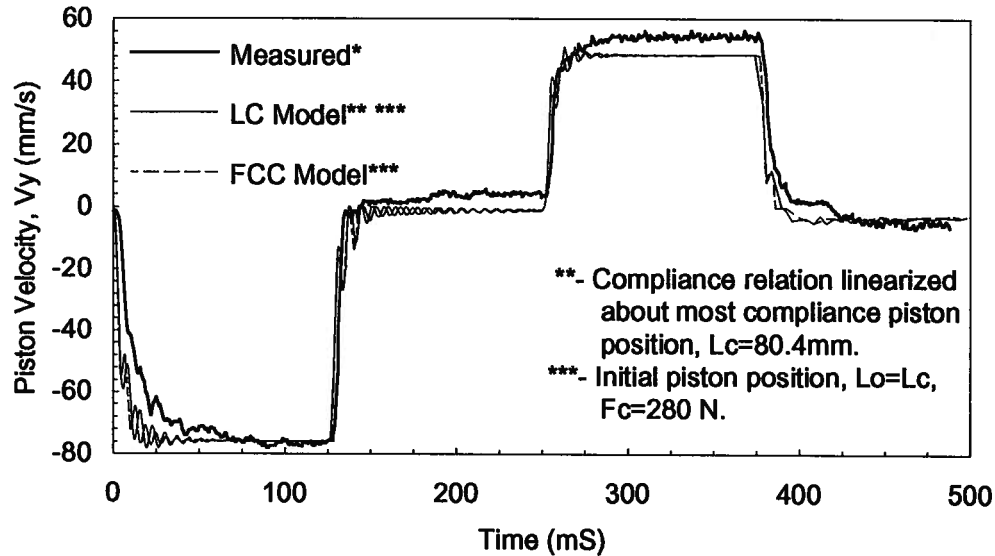


Figure 4.9. Comparison of the velocity response predicted by the LC and FCC models to the actual response.

Also, the actual system response is generally a bit slower than the response predicted by the models, particularly for the case when control valve is required to deliver more flow. While some of this sluggishness can be attributed to the aforementioned unmodeled piston seal leakage, the difference in response time exhibited between the valve opening and valve closing cases can be attributed to unmodeled flow non-linearities within the servovalve which cause its response time to be dependent upon the amplitude of the applied current.

Note that the steps in the velocity response of the actual system near the zero velocity can be attributed to valve deadband.

# 4.4 Conclusions

A model for the compliance of cylindrical actuators has been developed and applied. Both the supply system and the servo-actuator have been analyzed. The significant results of this analysis can be summarized as follows:

- Neglecting valve dynamics, symmetric actuators respond as second order systems with damping which is proportional to the amplitude of the valve opening.

- If the oil volume on each side of the piston is nearly equal, a second order model can also be used to represent the dynamics of an asymmetric actuator.

- Coulomb friction at the load tends to damp the actuator oscillations when the valve is in the critical position.

- A positioning system designed using linear theory should be analyzed for a range of piston positions.

# Chapter 5

# Identification of Servo-actuator Dynamics for Control

## 5.1 Introduction

While dynamic modeling is a useful tool for selecting hydraulic system components and determining the general order of the assembled system, the effects of valve deadband, hysteresis, stiction, spool leakage, and transport delay make the precise modeling of the dynamics of hydraulic systems difficult. To accommodate for these effects, a number of experiments can be conducted on the system in order to obtain a better representation of the system dynamics. These are known as system identification (SI) experiments and the practical result is an approximate linear model which can be used for the controller design. In this chapter, the three methods chosen to identify the system dynamics are discussed.

## 5.2   Choice of Identification Signal

Fundamentally, all system identification experiments involve two simple steps: 1) system input excitation and, 2) observation of the system response. Regardless of the type of SI experiment, the input signal used must be capable of exciting the relevant dynamics of the system. In order to choose an appropriate input excitation signal for a hydraulic system, some consideration must be given to practical limitations. For systems such as press brakes which position large masses, care must be taken to avoid potentially damaging excitation induced vibrations.

For a closed center spool valve, an investigation of the Improved Frequency Response (IFR) model reveals two important phenomena:

1. The response of a spool-valve controlled hydraulic cylinder becomes more damped as the amplitude of the input signal is increased.

2. The overall gain of the spool-valve is largest at the null flow position (all ports closed).

These two phenomena have led Merritt [14] to suggest that the null flow position, should be used for controller design. Since the null-flow position is the critical operating point for a position control system, it is reasonable to assume that the smaller the deviation from the null-flow position, the more relevant the identified model will be to the task of controller design. Further, the IFR model presented earlier shows that an equivalent linear frequency response model of the non-linear servo-actuator can be achieved if a periodic wave form of constant amplitude is used. Given this, a low amplitude periodic wave form with a mean amplitude of zero would seem to be ideal.

Unfortunately, valve deadband and hysteresis affect the valve dynamics most at the null position. Furthermore, the amplitude of the input signal has to be large enough so that the steady state flow gain identified is not biased by the valve-spool stiction. Parker and Desjardins [31] have suggested that a Pseudo Random Binary Sequence (PRBS) input signal of an amplitude of at least 10% of the maximum amplitude is sufficient to eliminate the effects of non-linear valve gain and spool friction. In practice, the amplitude of excitation signal required will vary with each system.

Watton [29] has shown that the steady state flow gain (SSFG) of an asymmetrical actuator extending will not be equal to the SSFG of the same actuator retracting. Furthermore, if significant Coulomb friction is present at the load, and the input excitation signal chosen causes the load to change direction, the system will undergo an external load excitation. Such system excitations are undesirable during identification experiments. Therefore, if accurate estimations of the steady-state velocity response of the actuator are to be obtained, separate identification experiments should be conducted for the extending and retracting cases.

## 5.3 System Response to a Step Input

In order to determine the velocity response of each actuator to a step change in valve command voltage, two sets of experiments were conducted: one in extension and one in retraction. For each experiment, an alternating step input signal of non-zero mean and not passing through zero voltage was applied to the servo-valve amplifier, and the velocity response of the load was measured. Each experiment was repeated for a number of differing input amplitudes.

The response of the hydraulic system to a typical step change in valve input signal during extension is shown in figure 5.1. Approximate first-order system parameters obtained from the step response experiments are presented in table 5.1. Note that the extension response differs somewhat from the retraction response. From this table we can
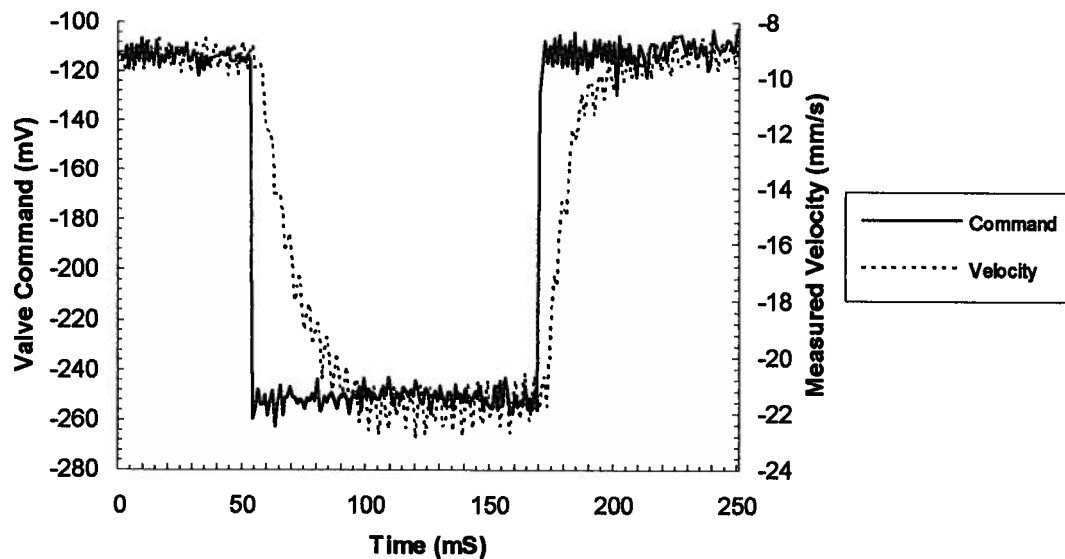


Figure 5.1. Velocity response of the left actuator to a step change in valve command voltage.

see that while the steady state velocity and delay do not change significantly with the amplitude of the excitation signal, the rise time does. Further, the rise time for the extending cases varies somewhat from that of the retracting cases.

| Left Actuator Extending | | Valve Opening | | Valve Closing | |
|---|---|---|---|---|---|
| Step Amp (V) | Gain (mm/V.s) | Rise (ms) | Delay (ms) | Rise (ms) | Delay (ms) |
| 0.100 | 7.93 | 12.0 | 5 | 9.2 | 4 |
| 0.150 | 9.53 | 15.0 | 4 | 7.9 | 4 |
| 0.250 | 9.48 | 12.5 | 4 | 7.8 | 3 |
| | | | | | |
| Left Actuator Retracting | | Valve Opening | | Valve Closing | |
| Step Amp (V) | Gain (mm/V.s) | Rise (ms) | Delay (ms) | Rise (ms) | Delay (ms) |
| 0.100 | 6.75 | 15.4 | 4 | 7.3 | 3 |
| 0.150 | 7.74 | 16.8 | 4 | 8.4 | 3 |
| 0.250 | 7.53 | 13.4 | 4 | 7.2 | 3 |
| | | | | | |
| Right Actuator Extending | | Valve Opening | | Valve Closing | |
| Step Amp (V) | Gain (mm/V.s) | Rise (ms) | Delay (ms) | Rise (ms) | Delay (ms) |
| 0.100 | 3.95 | 11.2 | 4 | 8.9 | 4 |
| 0.150 | 4.61 | 7.5 | 3 | 6.4 | 3 |
| 0.250 | 6.11 | 7.6 | 3 | 6.1 | 3 |
| | | | | | |
| Right Actuator Retracting | | Valve Opening | | Valve Closing | |
| Step Amp (V) | Gain (mm/V.s) | Rise (ms) | Delay (ms) | Rise (ms) | Delay (ms) |
| 0.100 | 5.80 | 6.1 | 4 | 5.9 | 4 |
| 0.150 | 6.00 | 5.8 | 4 | 5.8 | 3 |
| 0.250 | 6.03 | 6.2 | 4 | 6.1 | 3 |

Table 5.1. Delay, rise time and steady state gain obtained from step response experiments.

## 5.4 Frequency Response Experiments

### 5.4.1. Experiment Description

In order to determine the relevant dynamics of the system, frequency response experiments were conducted on each actuator for the extending and retracting cases. For each actuator, an input signal was applied to servo-valve input, and the velocity signal was measured. A PRBS input signal was selected because of the excellent signal to noise ratio effected in the velocity transducer. To minimize the effects of hysteresis, deadband, and coulomb friction loading, a DC offset was added to the signal to ensure the valve did not pass through the null position, reversing the direction of the load. Because the IFR model indicates that the frequency response of such hydraulic systems varies with the amplitude of the excitation signal, these experiments were conducted for a range of excitation signal amplitudes.

The data from each experiment was analyzed using a transfer function analysis.

### 5.4.2. Experimental Results

The magnitude and phase responses of the left actuator in extension is shown in figures 5.2 and 5.3. Note that the peaks at 60Hz for the lower amplitude signals are due to electrical noise observed in both the command signal as well as the transducer signal. From these results, a few observations can be made:

1. As the amplitude of the excitation signal is decreased, the steady-state gain of the system decreases as well. This can be attributed to the increased effect of valve component stiction at low valve actuation forces as discussed in [31].

2. The band pass frequency of the velocity loop is approximately 30 Hz. This compares favourably with the band pass predicted by LPLF model.
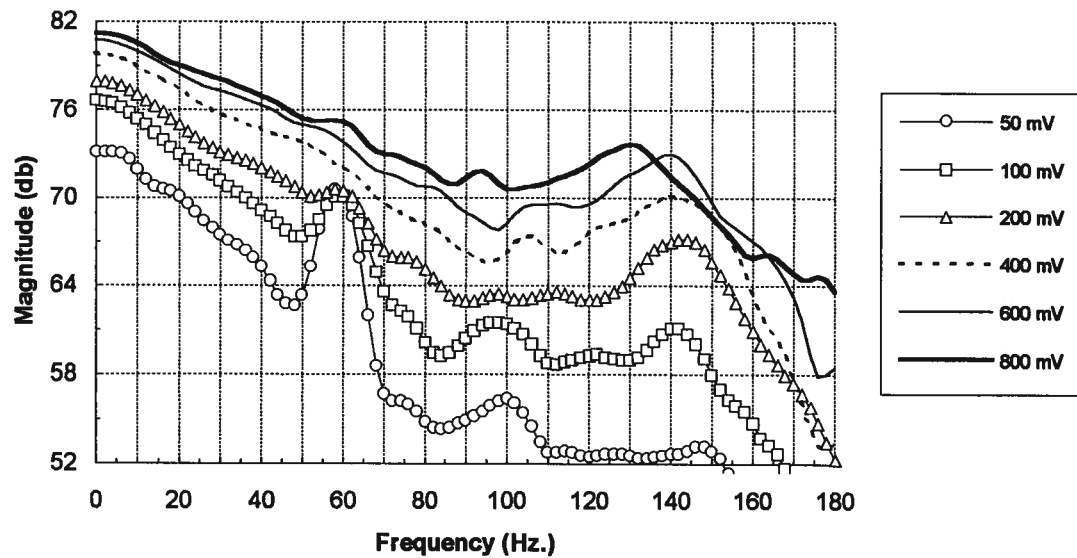
Figure 5.2. Magnitude response of the right actuator in extension determined for a variety of input signal amplitudes
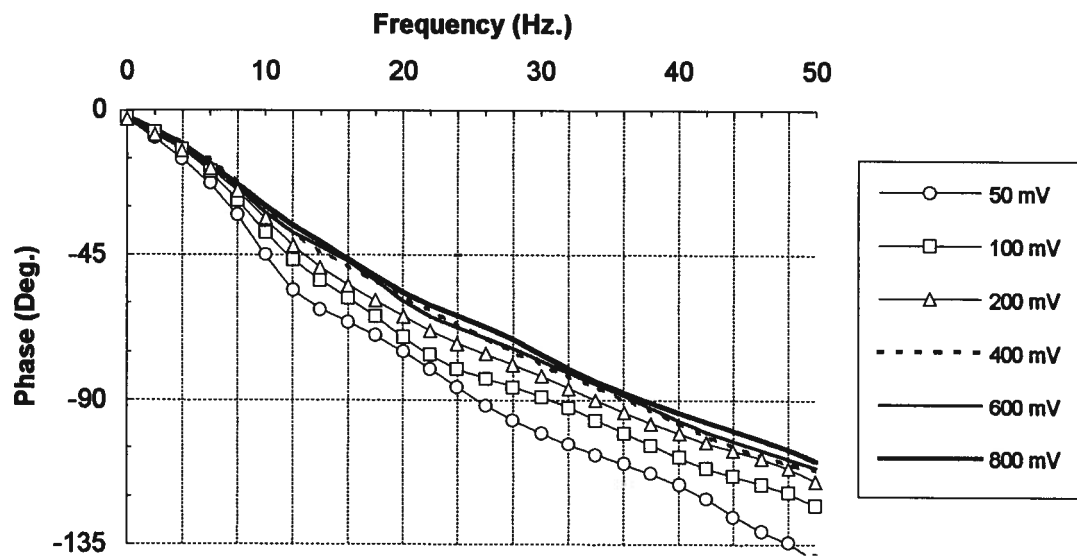


Figure 5.3. Phase response of left actuator in extension determined for a variety of input signal amplitudes

3. There exists a dynamic mode due to load dynamics near 140 Hz. As the amplitude of the input signal is increased, the frequency of this mode decreases. This frequency decrease can be attributed to an increase in valve damping as predicted by the IFR model.

4. At low amplitudes of input signal, the system exhibits a dynamic mode near 100 Hz. Since this mode disappears at higher amplitudes, it is likely caused by the higher order dynamics of the valve spool which, like the hydraulic cylinder, is underdamped only for small valve openings.

# 5.5 Parametric Identification

## 5.5.1 Theory

In order to determine a more precise description of the dynamic system model, a number of parametric identification experiments were conducted. Due to its ability to give unbiased estimates under less restrictive conditions, the Method of Instrumental Variables was chosen over the Least Squares Method to determine the model coefficients. A brief description of theses identification schemes follows.

Soderstrom and Stoica [32] present excellent descriptions of the Least Squares (LS) method as well as the Instrumental Variables (IV) method. Since the IV method is based on the LS method, it is useful to introduce the LS method first.

### 5.5.1.1 Least Squares Method

The discrete time transfer function for the open-loop velocity response of a hydraulics servo actuator has the form:

$$\frac{v_y(q^{-1})}{u(q^{-1})} = \frac{B(q^{-1})}{A(q^{-1})} \tag{5.1}$$

where

$$B(q^{-1}) = b_0 + b_1 q^{-1} + ... + b_{n_b} q^{-n_b}$$

$$A(q^{-1}) = 1 + a_1 q^{-1} + a_2 q^{-2} + .. + a_{n_a} q^{-n_a}$$ 

(5.2)

Using the Auto Regressive Moving Average (ARMA) notation, (5.1-5.2) can be reformulated as a time series

$$v_y(k) = b_0 u(k) + b_1 u(k-1) + ... + b_{n_b} u(k-n_b) - a_1 v_y(k-1) - ... - a_{n_a} v_y(k-n_a)$$ 

(5.3)

or

$$v_y(k) = \varphi^T(k)\theta$$ 

(5.4)

where:

$$\varphi(k) = \left( u(k)...u(k-n_b) \quad -v_y(k-1)... \quad -v_y(k-n_a) \right)^T$$ 

(5.5)

and

$$\theta = \left( b_0...b_{n_b} \quad a_1...a_{n_a} \right)^T$$ 

(5.6)

is the parameter vector of variables describing the 'true' dynamics of the system. The goal of the parametric identification is to obtain the parameter vector $\theta$ from a data set of $N$ measured regressors

$$\Phi = \begin{pmatrix} \varphi^T(1) \\ \vdots \\ \varphi^T(N) \end{pmatrix}$$ 

(5.7)

and the measured output

$$V_y = \begin{pmatrix} v_y(1) \\ \vdots \\ v_y(N) \end{pmatrix}$$ 

(5.8)

If a set of independent measurement errors with zero mean and variance $\lambda^2$ (white noise) exist such that:

$$E = \begin{pmatrix} \varepsilon(1) \\ \vdots \\ \varepsilon(N) \end{pmatrix} = \begin{pmatrix} v_y(1) - \varphi^T(1)\theta \\ \vdots \\ v_y(N) - \varphi^T(N)\theta \end{pmatrix} \qquad (5.9)$$

the least squares estimate of $\theta$ (denoted as $\hat{\theta}$), is that which minimizes the sum of the squares of the measurement errors:

$$V(\theta) = \frac{1}{2}\sum_{k=1}^{N}\varepsilon^2(k) \qquad (5.10)$$

It has been shown that if the loss function, (5.10) has a unique minimum, this minimum occurs for

$$\hat{\theta} = \left[\frac{1}{N}\sum_{k=1}^{N}\varphi(k)\varphi^T(k)\right]^{-1}\left[\frac{1}{N}\sum_{k=1}^{N}\varphi(k)v_y(k)\right] \qquad (5.11)$$

Note that in order for this minimum to exist, $\sum_{k=1}^{N}\varphi(k)\varphi^T(k)$ must be non-singular.

For this reason, care must be taken to choose an excitation signal which is 'persistently exciting'. In simpler terms, the input signal used to construct the data set must be capable of exciting the particular dynamics of the system one wishes to identify. Given that the above conditions hold, $\hat{\theta}$ has been shown to converge to $\theta$ for large $N$.

However, if the elements of the measurement error vector $\varepsilon$ are not linearly independent, $\hat{\theta}$ has been shown to converge to a biased estimate of $\theta$. Soderstrom and Stoica [32]present this phenomena as follows. If the true response of the system is given by

$$v_y(k) = \varphi^T(k)\theta + w(k) \qquad (5.12)$$

where $w(k)$ is stochastic disturbance, the difference between the true parameters and the estimated parameters can be written as:

$$\hat{\theta} - \theta = \left[\frac{1}{N}\sum_{k=1}^{N}\varphi(k)^T\varphi(k)\right]^{-1}\left[\frac{1}{N}\sum_{k=1}^{N}\varphi(k)^T w(k)\right] \qquad (5.13)$$

As the number of samples $N$ tends towards infinity, equation (5.13) will not converge to zero unless the expectation

$$E\varphi(k)^T w(k) = 0 \qquad (5.14)$$

If a correlation exists between the measurement error and the regression vector, 5.14 will fail. While this bias may be small for systems with a high signal to noise ratio, other methods, such as the Instrumental Variable method have been shown to provide unbiased estimates in the presence of correlated measurement errors.

## 5.5.1.2 Instrumental Variables Method

The IV method augments the LS method by the introduction of a vector of signals or 'instruments'

$$Z(k) = \left( u(k)...u(k-n_b) \quad \eta_y(k\text{-})...\eta_y(k-n_a) \right)^T \qquad (5.15)$$

which are uncorrelated to the disturbance $w(k)$. Note that the instruments:

$$\left[ \eta_y(k\text{-})...\eta_y(k-n_a) \right] \qquad (5.15)$$

are determined from the measured output. Thus the function to be minimized becomes:

$$V(\theta) = \frac{1}{2}\sum_{k=1}^{N}\left( Z(k)^T \varepsilon(k) \right)^2 \qquad (5.16)$$

and the IV estimate of the parameter vector is:

$$\hat{\theta}_{iv} = \left[ \sum_{k=1}^{N} Z(k)\varphi^T(k) \right]^{-1}\left[ \sum_{k=1}^{N} Z(k)v_y(k) \right]^T \qquad (5.17)$$

The determination of the instruments involves filtering of the measured output and therefore requires an *a priori* estimation of the stochastic disturbance term $w(k)$. Typically this estimation is performed on an independent data set using the LS method. For this reason, IV methods require a significant amount more computation time than simple LS methods.

The approximately optimal IV method was chosen to identify the dynamic system parameters in this experiment. For a detailed description of this method see Soderstrom and Stoica [32].

## 5.5.2. Experiment Description

For this experiment, a small amplitude excitation signal was applied to the servo-valve amplifier. This excitation signal as well as an output voltage from the velocity transducer was sampled at 1 millisecond intervals. The collected data was analyzed using Matlab's System Identification Toolbox [33]. Experiments were conducted for each actuator extending and retracting.

### 5.5.2.1 Choice of Identification Signal

Of the two types of signal considered, pseudo random noise and a pseudo-random binary sequence (PRBS), the PRBS was chosen because of the superior signal to noise ratio effected in the velocity transducer. A DC bias (as in the frequency response experiment) was added to the PRBS to prevent reversing the direction of the load. In order to determine the lowest amplitude signal capable of minimizing the non-linear valve characteristics a number of frequency response experiments were conducted using excitation signals of differing amplitudes.

The open-loop velocity gain predicted for each amplitude of input signal applied for the left actuator in extension is shown in figure 5.4

At low input signal amplitudes, the velocity response is dominated by valve non-linearities. As the amplitude of the excitation signal is increased, more consistent estimates of the open loop gain are obtained. From these experiments, an input signal amplitude of 600mV, or 3% of the maximum valve input, was chosen. This amplitude, the

lowest input signal amplitude capable of overcoming the valve stiction, was within the range of input signals required during the forming operation.
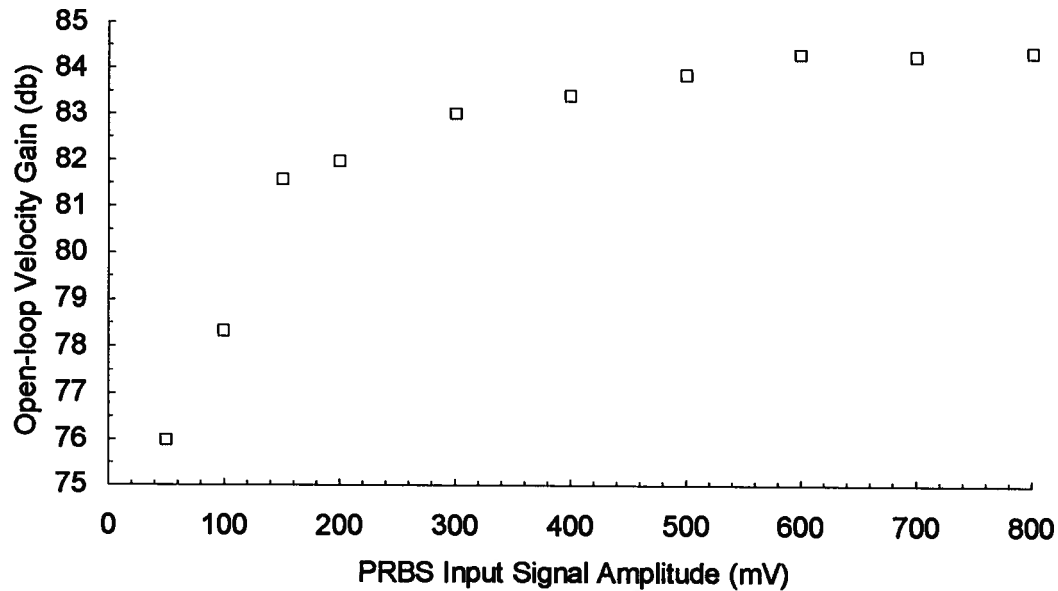


Figure 5.4. Effect of excitation signal amplitude on the steady-state gain predicted by the frequency response experiments (left actuator extending).

## 5.5.2.2 Model Structure

In order to effectively determine the dynamics system parameters using the parametric identification techniques described above, information about the model structure must be known. From the frequency response analysis, the third order system dynamics predicted by the IFR model can be observed: a dominant first order lag due to the valve dynamics combined with slight oscillatory mode due to the actuator/load dynamics. From the step response analysis, a first order response with 3-4 ms delay can be observed.

## 5.5.2.3 Data Analysis

For each situation (left actuator extending, left actuator retracting, right actuator extending, right actuator retracting) a number of trials were conducted. For each trial the servo-valve command and the voltage across the velocity transducer were sampled at 1 millisecond intervals. The 4000 point data sets collected were split into two 2000 point data sets: the first was used for estimation of the dynamics system parameters, the second to validate the estimated model.

For each identification data set, the 'approximately optimal' IV method was applied for a number of model structures of first and third orders with two to five milliseconds of delay. Using the validation data set, the response for each identified model was compared to the actual system response. A prediction error function consisting of the sum of the squares of the error between the actual system response and the simulated response was computed to compare the relative goodness of fit for each model.

## 5.5.3. Experimental Results
## 5.5.3.1 Model Selection

A comparison of the loss functions for each structure of model fit to the data is presented in Table 5.2. The structures corresponding to the minimum value of loss function are shown highlighted.

The identified model parameters for the candidate structures are presented in Table 5.3. Note that model parameters for two alternate candidate structures pertaining to the extension cases have been included.

| Model $\dfrac{B(q^{-1})}{A(q^{-1})} = q^{-n_d} \dfrac{b_0 + b_1 q^{-1} + \cdots + b_{n_b} q^{-n_b}}{1 + a_1 q^{-1} + \cdots + a_{n_a} q^{-n_a}}$ | | | Loss Function | | | |
|---|---|---|---|---|---|---|
| | | | Left Actuator | | Right Actuator | |
| $n_a$ | $n_b$ | $n_d$ | Extending | Retracting | Extending | Retracting |
| 1 | 1 | 2 | 2065 | 2376 | 814 | 620 |
| 1 | 1 | 3 | 718 | 1394 | 603 | 492 |
| 1 | 1 | 4 | 1084 | 2133 | 621 | 1052 |
| 1 | 1 | 5 | 1734 | 2936 | 1083 | 2553 |
| 1 | 1 | 6 | 2036 | 3021 | 1876 | 3408 |
| 3 | 3 | 2 | 1495 | 3275 | 260 | 1482 |
| 3 | 3 | 3 | 234 | 219 | 353 | 149 |
| 3 | 3 | 4 | 54 | 80 | 118 | 112 |
| 3 | 3 | 5 | 205 | 155 | 548 | 298 |
| 3 | 3 | 6 | 467 | 605 | 1104 | 627 |

Table 5.2. Comparison of the loss functions computed for a variety of model structures.

### 5.5.3.2 Model Validation

In order to ensure that the identified parameters are reasonably accurate descriptions of the relevant system dynamics, two sets of validation experiments were conducted: a frequency response comparison and step response comparison.

For the first comparison, the frequency response predicted by each of the candidate models for each case was compared to the frequency response determined directly from sampled data.

The measured frequency response of the left actuator extending is compared to that predicted by the identified candidate models in figure 5.5. Although overestimating the steady state gain, the first order model with three sampling delays gives an excellent description of the process dynamics for frequencies between 10 and 65 Hz. The first order model with four delays accurately predicts the steady state gain, but generally over estimates the response of the system for frequencies between 10 and 110 Hz. The third order model with four delays is capable of representing the dynamics mode due to the

load/actuator dynamics, but the amplitude at the resonant mode is significantly

overestimated.

| Case | $n_a$ | $n_b$ | $n_d$ | $[A] = 1 + a_1 q^{-1} + \cdots + a_{n_a} q^{-n_a}$ | $[B] = b_0 + b_1 q^{-1} + \cdots + b_{n_b} q^{-n_b}$ |
|---|---|---|---|---|---|
| Left Extension | | | | | |
| | 1 | 1 | 3 | [1, -0.9197] | [704.9, 920.6] |
| | 1 | 1 | 4 | [1, -0.8712] | [1572.7, 702.44] |
| | 3 | 3 | 4 | [1, -2.057, 1.885, -0.7661] | [1890.6, -1813.5, 1120.4, -206] |
| Right Extension | | | | | |
| | 1 | 1 | 3 | [1,-0.9170] | [738.0, 417.1] |
| | 1 | 1 | 4 | [1, -0.8609] | [982.3, 505.3] |
| | 3 | 3 | 4 | [1, -1.9342, 2.4757, -1.3156] | [1335.8, -361.65, -308.06, 1760.7] |
| Left Retraction | | | | | |
| | 1 | 1 | 3 | [1, -0.9022] | [699.2, 657.3] |
| | 3 | 3 | 4 | [1, -2.0982, 1.9283, -.7785] | [448.5, 1204.5, -1676] |
| Right Retraction | | | | | |
| | 1 | 1 | 3 | [1, -0.8558] | [1111, 558.3] |
| | 3 | 3 | 4 | [1, -2.1225, 2.0106, -0.8145] | [2131, -2808 2361 -818.4] |

Table 5.3. Model Parameters determined from parametric identification

The measured frequency response of the right actuator extending is compared to

that predicted by the identified candidate models in figure 5.6. The first order model with

three sampling delays tends to overestimate the response of the system from steady state

to 15 Hz, while underestimating it everywhere else. The first order model with four delays

accurately predicts the steady state gain, gives a reasonably accurate description of the

response of the system for frequencies between 0 and 100 Hz. The third order model with

four delays gives a reasonable description of the system dynamics from steady state to 90

Hz, although it incorrectly predicts the dynamic mode.

The measured frequency response of the left actuator retracting is compared to

that predicted by the identified candidate models in figure 5.7. While both models

accurately predict the steady-state gain of the system, the third order model with four

delays better represents the dynamics throughout the range of frequencies. Note however
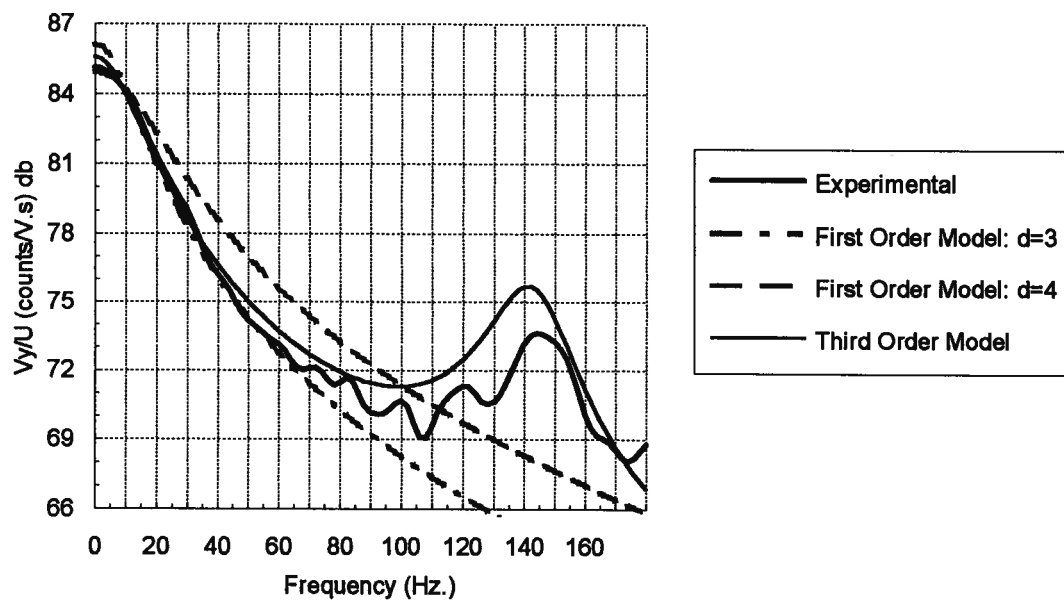
Figure 5.5. A comparison of the experimentally determined frequency response to that predicted by the identified models: Left actuator extending.
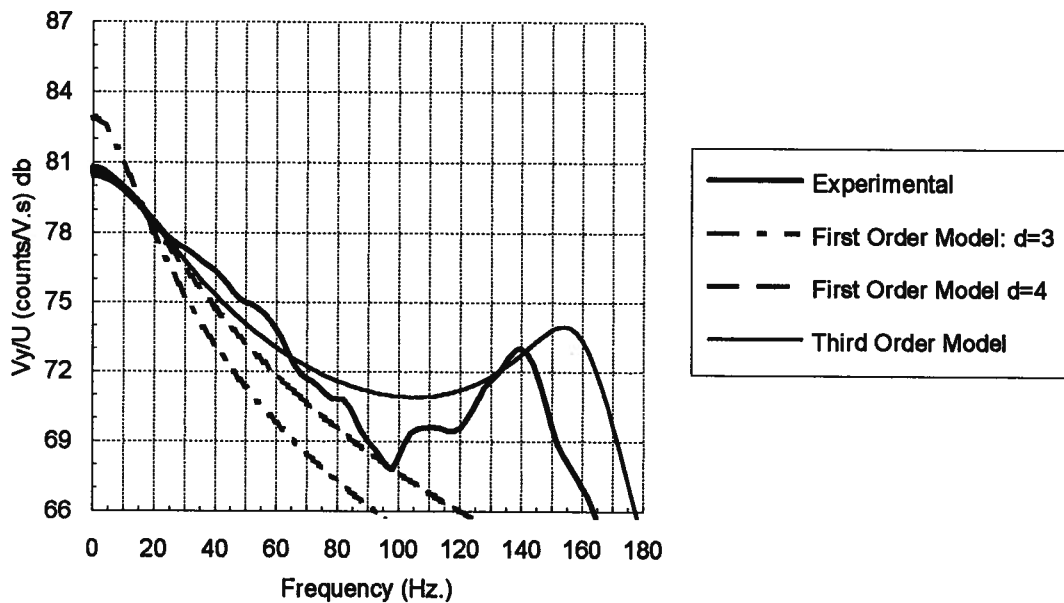


Figure 5.6. A comparison of the experimentally determined frequency response to that predicted by the identified models: Right actuator extending.

the third order model dramatically overestimates the frequency response of the dynamic mode.
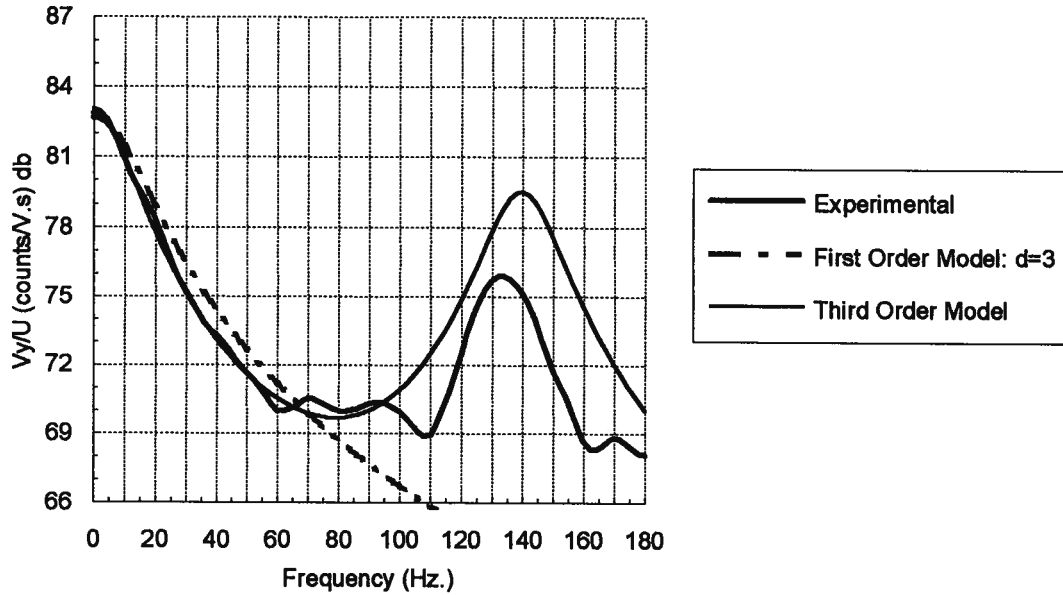


Figure 5.7. A comparison of the experimentally determined frequency response to that predicted by the identified models: Left actuator retracting.

The measured frequency response of the right actuator extending is compared to that predicted by the identified candidate models in figure 5.8. The first order model gives a good description of the response of the system from steady state through to 85 Hz. The third order model gives a good description of the system dynamics from steady state up to 60 Hz, but beyond this gives an poor estimate of the dynamics and incorrectly predicts the of the dynamic mode.

For the step response comparison, the response predicted by each of the candidate models for each case was compared to a measured response from a data set independent of that used in the identification.
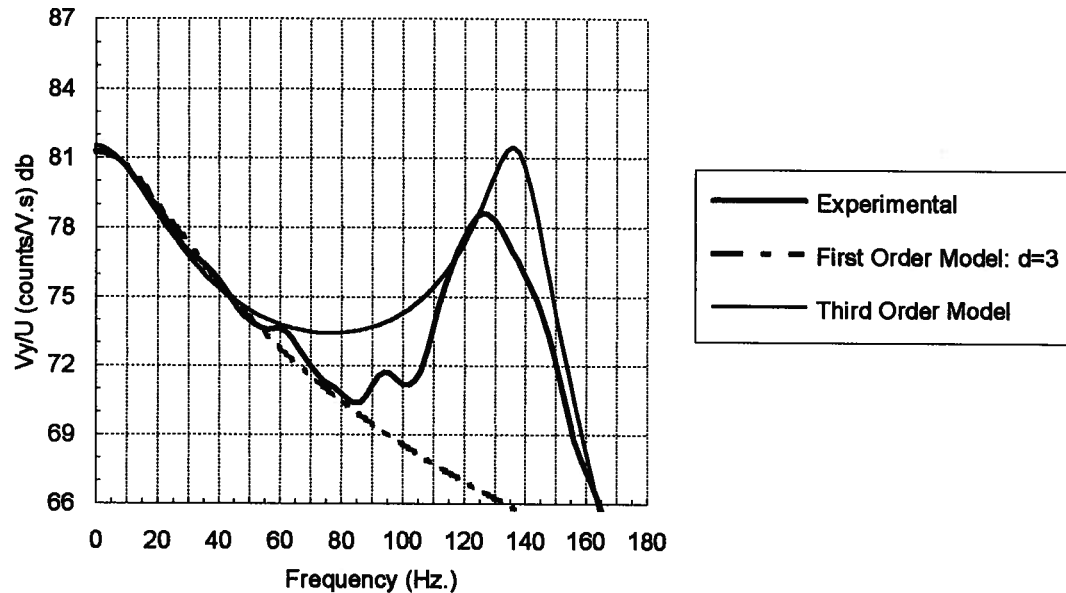
Figure 5.8. A comparison of the experimentally determined frequency response to that predicted by the identified models: Right actuator retracting.

The measured response of the left actuator extending is compared to that predicted by the identified candidate models in figure 5.9. While none of the models tested constitutes an excellent fit, the third order model seems to give the best representation of the dynamics and the steady-state gain. Both first order models give reasonable fits with neither being outstanding at all points on the comparison.

The measured response of the right actuator extending is compared to that predicted by the identified candidate models in figure 5.10. Again, while none of the models tested constitutes an excellent fit, the third order model seems to give the best representation of the dynamics and the steady-state gain. The first order model with four delays predicts a response very similar to the third order model, but without the higher-order dynamics. The first order model with three delays tends to overestimate the steady-state gain while underestimating the rise time of the system.
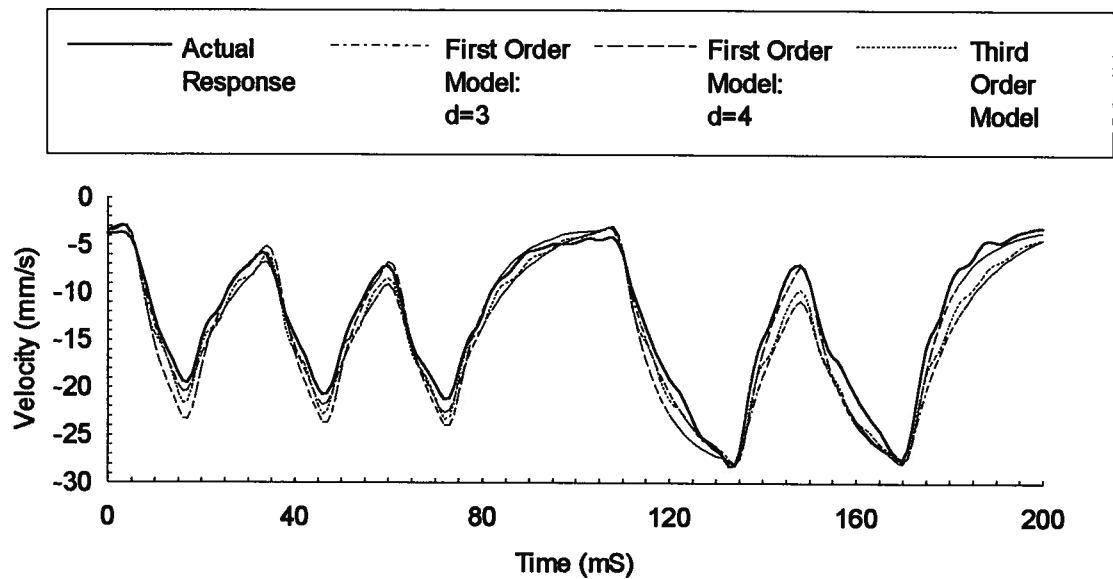
Figure 5.9. Comparison of the response of the measured system to that predicted by the parametrically identified models: left actuator extending.

The measured response of the left actuator retracting is compared to that predicted by the identified candidate models in figure 5.11. In this case, the system is exhibiting third order or higher dynamics. Although a slight DC bias seems to exist, the third order model gives the best fit. The response predicted by the first order model with three delays seem to fit the first order dynamics satisfactorily despite the same DC bias.

The measured response of the right actuator retracting is compared to that predicted by the identified candidate models in figure 5.12. As was the case with the left actuator retracting, the system response is clearly third order or higher with a higher mode frequency of approximately 135 Hz. While generally underestimating the amplitude of the higher order oscillations, the response predicted by the third order model does fit the actual response reasonably well. Again, the response predicted by the first order model with three delays seems to fit the first order dynamics as well as can be expected.
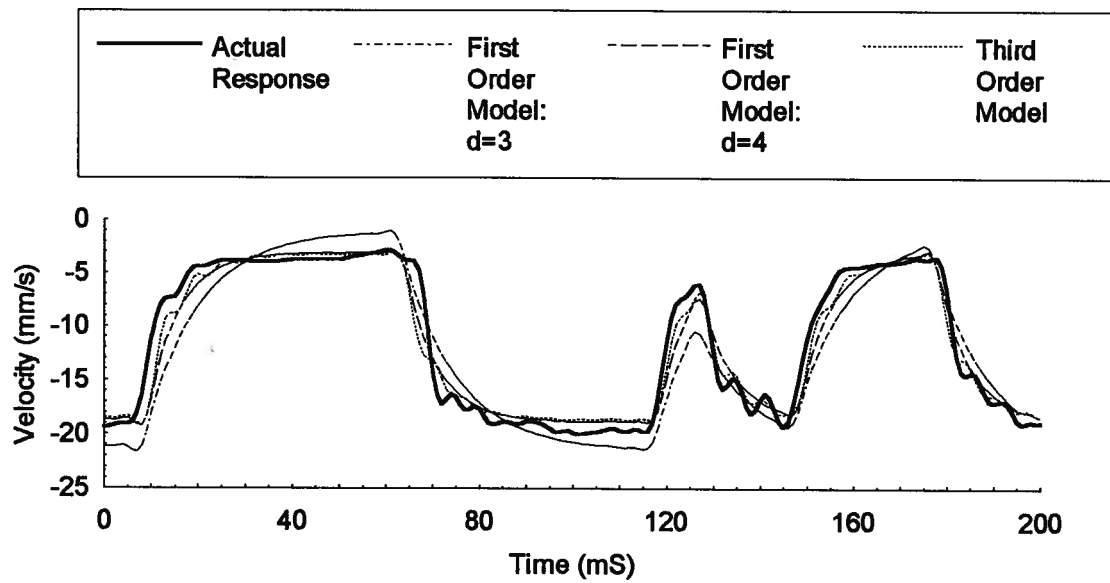
Figure 5.10. Comparison of the measured system to that predicted by the parametrically identified models: right actuator extending.
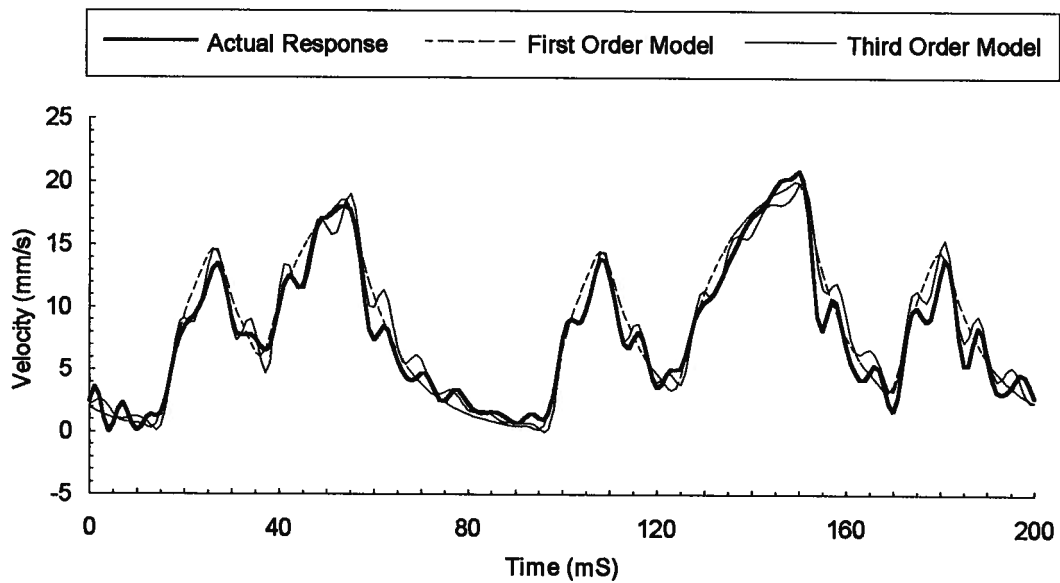


Figure 5.11. Comparison of the measured system to that predicted by the parametrically identified models. Left actuator retracting.
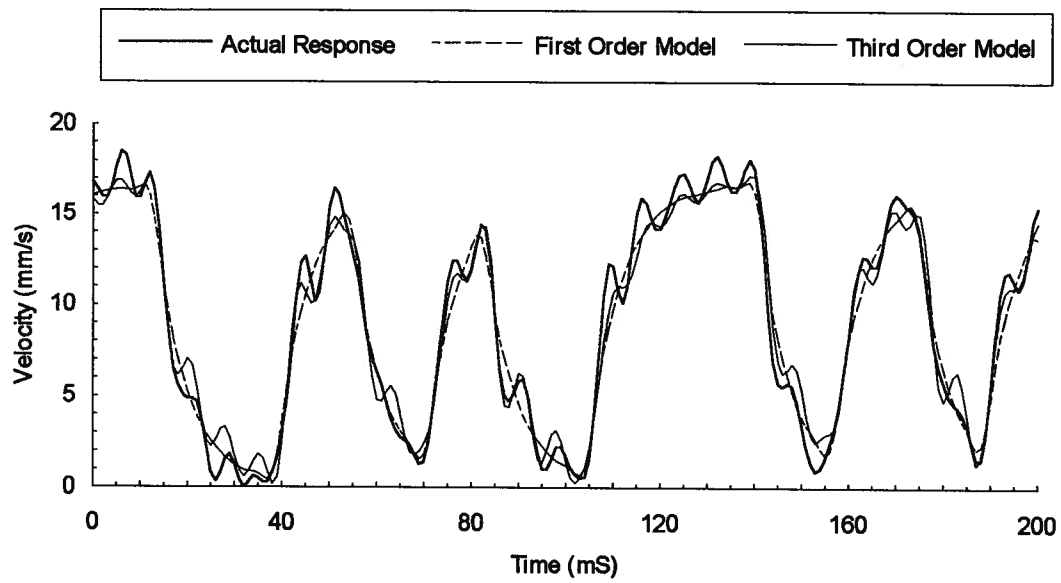
Figure 5.12. Comparison of the measured system to that predicted by the parametrically identified models: right actuator retracting.

## 5.6 Conclusion

From the identification experiments a number of conclusions can be drawn:

- At very small input signals, the steady state gain of the servo-actuator drops significantly and the dynamics of the load are not significant.

- As the amplitude of the input signal is increased, the steady-state gain of the servo-actuator increases and an oscillatory mode at 130-150 Hz due to the load dynamics is more apparent.

- The system response of the servo-actuators in the extending cases can be represented adequately by a first order model.

- The response of the servo-actuators in the retracting cases can be characterized by a dominant first order lag combined with a low amplitude dynamic mode at approximately 130-150 Hz.

# Chapter 6

# Coordinated Motion Control of Press Ram

## 6.1 Introduction

The objective of the efforts described in this chapter was to design and implement a practical control scheme which accomplished smooth positioning and orientation of the punch with respect to the die throughout the bend cycle. In order to facilitate coordinated motion between the two actuators, a control scheme capable of matching the closed loop positioning dynamics of the axes was chosen. Model parameters presented in the previous chapter were used exclusively for the controller design.

Given the cost sensitivity of manufacturing a machine tool for the industrial market, efforts to improve the positioning performance focused on software rather than on hardware. Although velocity and pressure signals were available and could have improved the robustness and performance of the system, only position feedback was used so that the incremental cost of CNC implementation would be less. The results indicate that as long as the control law is properly designed, the system behaves satisfactorily without pressure and velocity feedback signals.

In this chapter, the term 'following error' refers to the difference between the desired position and the actual position of either axis during movement at a particular velocity. The term 'tracking error' has been used to describe the difference between following error of each axis. The term 'steady-state-positioning error' refers to the difference between the desired position and the actual position of either axis when the desired position is not changing and system dynamics are not prevalent.

# 6.2 Motion Control

## 6.2.1. Objective

The motion control task attempted to achieve two fundamental objectives:

1. less than 0.25 mm tracking error during the forming process

2. a steady-state positioning error of less than 0.015 mm under forming load.

## 6.2.2. Velocity Profile

A plot of the desired punch velocity profile for a brake-forming cycle is depicted in figure 6.1. The profile consists of four segments:

1. rapid approach to the clearance plane above the work-piece

2. brake-forming operation at feed-rate

3. dwell in bend

4. rapid retract to the start position
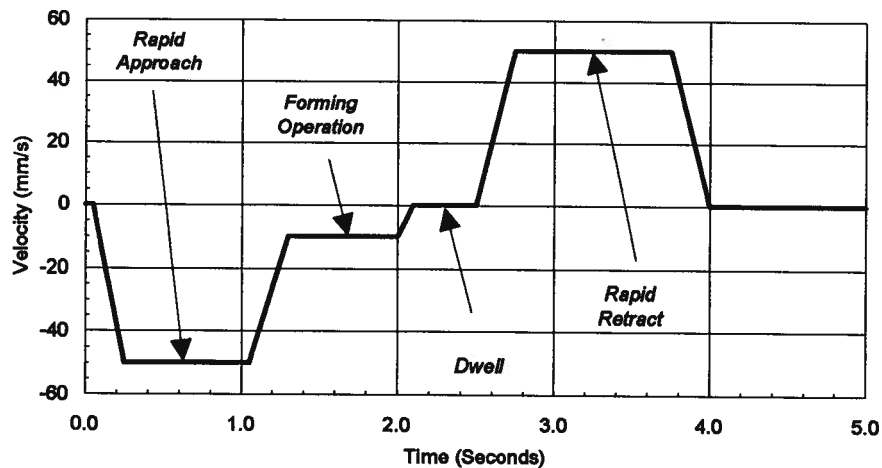
Figure 6.1. Velocity profile for typical bending cycle.

The performance of the positioning system during the bend and dwell operations determines the precision of the press. In these cases, the actuators are either extending or

holding their position against a forming load. For these reasons, the actuator models corresponding to the extension cases were used for controller design.

### 6.2.3. The Process to be Controlled

The results of the identification experiments have shown that the response of the actuators can be characterized by a first order lag combined with an under damped mode at approximately 140 Hz. However, for the extension cases, the higher order dynamics are less prevalent especially for the small input signal amplitudes (100-150 mV) used during the forming operation. Moreover, the first order models generally provide good descriptions of the dynamic system performance at frequencies up to 100 Hz. Furthermore, considering the computational complexity required to compensate for higher order dynamics, the first order models were chosen for initial design efforts.

### 6.2.4 Control Scheme

### 6.2.4.1 Introduction

In order to achieve low tracking error, a control scheme which would facilitate matching the dynamics of each positioning system was desirable. In order to obtain low steady-state position error, the closed loop positioning system would require high gain to maximize load force disturbance rejection. Since the open-loop system dynamics contained several delays, a delay compensation scheme was deemed necessary to allow high controller gain. A pole-placement control scheme, similar to that used by Watton [22] was chosen because it utilizes a performance-based design procedure and is capable of compensating for process delays.

A block diagram of a pole-placement controlled system is shown in figure 6.2. The process to be controlled is represented by polynomials of open loop system zeros $B$ and the poles $A$. The controller consists of a feed-forward filter $T$, a feed-back filter $S$,

controller poles $R$ and an estimation filter (or observer) $A_0$. These four filters are selected such that the controlled system responds according to a chosen response:
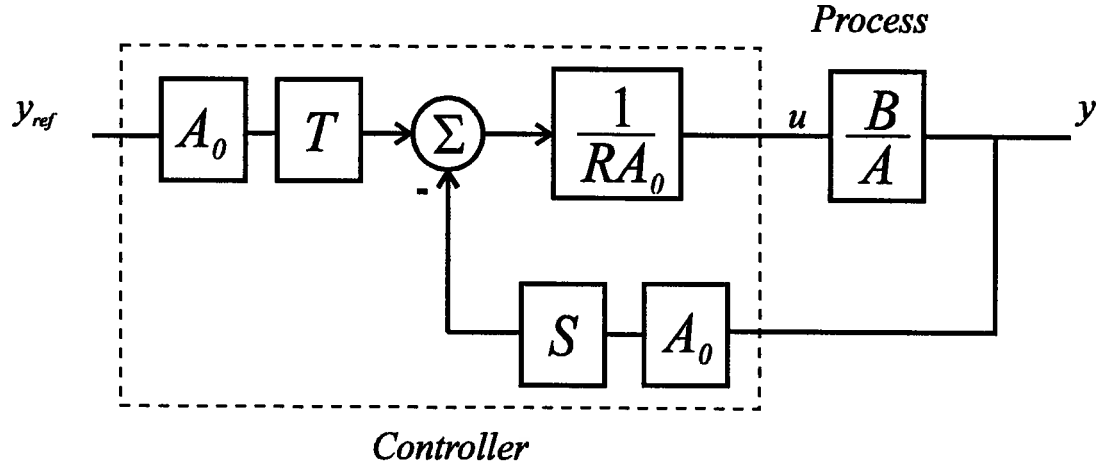


Figure 6.2. Block diagram of a pole-placement controlled system.

$$\frac{y}{y_{ref}} = \frac{BT}{AR + BS} = \frac{B_m}{A_m}$$

(6.1)

where $A_m$ contains the poles, and $B_m$ the zeros of the desired closed loop transfer function (CLTF).

A detailed description of the pole-placement design process can be found in [34]. A description of how the pole-placement control scheme was adapted to the position control task follows.

### 6.2.4.2 Design of the Pole-Placement Controller

The open-loop velocity response of each of the servo-actuators in the extending cases can be represented by the following discrete time transfer function:

$$\frac{v_y(q^{-1})}{u(q^{-1})} = \frac{q^{-n_d}(b_0' + b_1'q^{-1})}{1 + a_1'q^{-1}} \quad \left[\frac{\text{counts}}{\text{V} \cdot \text{sec}}\right] \tag{6.2}$$

where $n_d$ is the number of delays, $b_1'$, $b_2'$, and $a_1'$ are the identified system parameters, and 1 count/second equals 0.005mm/s of actuator velocity.

Adding an integration term to this expression yields:

$$\frac{y(q^{-1})}{u(q^{-1})} = \frac{q^{-n_d}(b_1 + b_2 q^{-1})}{(1 + a_1 q^{-1} + a_2 q^{-2})} \quad \left[\frac{\text{counts}}{\text{V}}\right] \tag{6.3}$$

or, for convenience, using the forward shift operator:

$$\frac{y(q)}{u(q)} = \frac{(b_1 q + b_2)}{q^{n_d}(q^2 + a_1 q^1 + a_2)} \quad \left[\frac{\text{counts}}{\text{V}}\right] \tag{6.4}$$

The desired system response was chosen to be that of a damped second order system with a delay equivalent to the open-loop system delay:

$$\frac{y(q)}{y_{ref}(q)} = \frac{B_m(q)}{A_m(q)} = \frac{(b_1 q + b_2)b_{m0}}{q^{n_d}(q^2 + a_{m1}q^1 + a_{m2})} \quad \left[\frac{\text{counts}}{\text{count}}\right] \tag{6.5}$$

where $y_{ref}(q)$ is the reference position, and $b_{m0}$ is gain chosen such that the position control loop has a unity steady state gain:

$$b_{m0} = \frac{1 + a_{m1} + a_{m2}}{b_1 + b_2} \tag{6.6}$$

Since it is desirable to use only the position transducers for process feedback, an observer $A_0(q)$ is required to estimate any higher order feedback terms required. In order to ensure a causal design analysis, Astrom and Wittenmark [34] have shown that the following conditions must be met:

$$\deg A_0(q) \geq 2\deg A(q) - \deg A_m(q) - 1 \tag{6.7}$$

$$\deg R(q) \geq \deg S(q) \tag{6.8}$$

$$\deg R(q) \geq \deg T(q) \tag{6.9}$$

$$\deg S(q) < \deg A(q) \tag{6.10}$$

$$\deg R(q) \geq \deg A_0(q) + \deg A_m(q) - \deg A(q) \tag{6.11}$$

Therefore, given (6.7) the order of the observer polynomial was chosen:

$$\deg A_0(q) = n_d + 1 \tag{6.12}$$

Since the linear encoders provide low-noise position measurements, the observer polynomial poles were placed at the origin for the fastest estimation convergence:

$$A_0(q) = q^{n_d+1} \tag{6.13}$$

In order to meet causality constraints (6.7-6.11) the controller polynomial orders were chosen such that:

$$\deg R(q) = \deg S(q) = \deg T(q) = n_d + 1 \tag{6.14}$$

Therefore, the controller polynomials were chosen to be:

$$R(q) = q^{n_d+1} + r_1 q^{n_d} + \cdots + r_{n_d} q^1 + r_{n_d+1} \tag{6.15}$$

$$S(q) = s_0 q^{n_d+1} + s_1 q^{n_d} + \cdots + s_{n_d} q^1 + s_{n_d+1} \tag{6.16}$$

$$T(q) = t_0 q^{n_d+1} + t_1 q^{n_d} + \cdots + t_{n_d} q^1 + t_{n_d+1} = b_{m0} A_0(q) = b_{m0} q^{n_d+1} \tag{6.17}$$

Solving the Diophantine equation symbolically for the controller parameters (Appendix B) yields:

$if(n_d = 1)$,

$$r_1 = a_{m1} - a_1 \tag{6.18}$$

$$r_2 = \frac{a_{m2} - \left(a_1 \dfrac{b_2}{b_1} - a_2\right) r_1 + a_2 \dfrac{b_2}{b_1}}{a_1 - a_2 \dfrac{b_1}{b_2} - a_0 \dfrac{b_2}{b_1}} \tag{6.19}$$

$$s_0 = -\frac{(r_2 + a_1 r_1 + a_2 - a_{m2})}{b_1} \tag{6.20}$$

$$s_1 = -\frac{a_2 r_2}{b_2} \tag{6.21}$$

$$s_i = 0, \quad i = 2,3,\cdots n_d + 1 \tag{6.22}$$

*if* $(n_d > 1)$,

$$r_1 = a_{m1} - a_1 \tag{6.23}$$

$$r_2 = a_{m2} - a_2 - a_1 r_1 \tag{6.24}$$

$$\text{for } j > 2, j \le n_d, \qquad r_j = -\left(a_1 r_{j-1} + a_2 r_{j-2}\right) \tag{6.25}$$

$$r_{n_d+1} = \frac{\left(\left(a_1\frac{b_2}{b_1} - a_2\right)r_{n_d} + a_2\frac{b_2}{b_1}r_{n_d-1}\right)}{\left(a_1 - a_2\frac{b_1}{b_2} - a_0\frac{b_2}{b_1}\right)} \tag{6.26}$$

$$s_0 = -\frac{\left(r_{n_d+1} + a_1 r_{n_d} + a_2 r_{n_d-1}\right)}{b_1} \tag{6.27}$$

$$s_1 = -\frac{a_2 r_{n_d+1}}{b_2} \tag{6.28}$$

$$s_i = 0, \quad i = 2,3,\cdots n_d + 1 \tag{6.29}$$

### 6.2.4.3 Controller Implementation

Using the forward shift notation, the pole-placement control law can be represented by:

$$R(q)u(q) = T(q)y_{ref}(q) - S(q)y(q) \tag{6.30}$$

Rewriting 6.30 using discrete time series notation yields:

$$u(k) = \sum_{l=0}^{n_t} t_l y_{ref}(k-l) - \sum_{i=0}^{n_s} s_i y(k-i) - \sum_{j=1}^{n_r} r_j u(k-j) \tag{6.31}$$

where $n_t$, $n_s$ and $n_r$ are the respective orders of the feed-forward, feed-back and controller polynomials. Given that in the applied case, $n_t = 0$, $n_s = 1$ and $n_r = n_d + 1$, the control law:

$$u(k) = t_0 y_{ref}(k) - \sum_{i=0}^{1} s_i y(k-i) - \sum_{j=1}^{n_d+1} r_j u(k-j) \tag{6.32}$$

would require $(n_d + 4)$ multiplication operations and $(n_d + 4)$ add operations per loop closure. Note that this implementation requires precise representation of parameters $t_0$, $s_0$ and $s_1$ in order to avoid steady-state error due to numerical round-off. For this reason, the following simplification was developed.

The steady state gain of a pole-placement controlled system can be represented by the following relation:

$$\frac{y(1)}{y_{ref}(1)} = \frac{\sum_{i=0}^{n_b} b_i \sum_{j=0}^{n_t} t_j}{\sum_{i=0}^{n_a} a_i \sum_{j=0}^{n_r} r_j + \sum_{i=0}^{n_b} b_i \sum_{k=0}^{n_s} s_k} = \frac{\sum_{i=0}^{n_{b_m}} b_{m_i}}{\sum_{j=0}^{n_{a_m}} a_{m_j}} \tag{6.33}$$

For systems with an inherent integration such as DC motor positioning systems or servo-hydraulic positioning systems

$$\sum_{i=0}^{n_a} a_i = 0$$

Therefore, (6.33) reduces to:

$$\frac{y(1)}{y_{ref}(1)} = \frac{\sum_{j=0}^{n_t} t_j}{\sum_{k=0}^{n_s} s_k} = \frac{\sum_{i=0}^{n_{b_m}} b_{m_i}}{\sum_{j=0}^{n_{a_m}} a_{m_j}} \tag{6.34}$$

which indicates that the steady-state gain of the pole-placement controlled system can be scaled by appropriate choices of $S$ and $T$. Furthermore, if the desired steady state gain is unity, then:

$$\sum_{j=0}^{n_t} t_j = \sum_{k=0}^{n_s} s_k, \tag{6.35}$$

For $n_t = 0$ and $n_s = 1$, 6.35 can be rewritten:

$$\sum_{i=0}^{1} s_i = t_0,$$ (6.36)

Substituting the relation:

$$\Delta y(k) = y(k) - y(k-1)$$ (6.37)

into the control law (6.32) and rearranging yields:

$$u(k) = t_0 y_{ref}(k) - \left(\sum_{i=0}^{1} s_i\right) y(k-1) - s_0 \Delta y(k) - \sum_{j=1}^{n_d+1} r_j u(k-j)$$ (6.38)

Using (6.36), the control law can be further simplified to yield:

$$u(k) = t_0 \left(y_{ref}(k) - y(k-1)\right) - s_0 \Delta y(k) - \sum_{j=1}^{n_d+1} r_j u(k-j)$$ (6.39)

which, in comparison with (6.32), requires only $(n_d + 3)$ multiplication operations and

$(n_d + 3)$ add operations per loop closure. This control law implementation (6.39)

accomplishes the following:

- it eliminates the possibility of the steady-state error due to numerical round-off during

  scaling computations while guaranteeing appropriately scaled output

- it reduces the number of control parameters that need to be represented, lessening

  memory requirements

- it reduces the precision in which $t_0$ and $s_0$ need to be represented, further lessening

  memory requirements

- it reduces the number and complexity of operations required for implementation

This control algorithm was implemented on two axes of the HOAM-CNC using

Intel 80196 assembly language. A pair of overdamped CLTF poles $(A_m)$ were chosen

such that the system response was fast enough to satisfy the following-error constraints

while not deviating significantly from the control valve dynamics. The control law

parameters as well as the process parameters used for design are shown in tables 6.1 and

6.2.

| Left Axis (Y1) | Pole-Placement Design Parameters | | | | | |
|---|---|---|---|---|---|---|
| $[B] = b_0 + b_1 q^{-1}$ | 1573 | 702 | | | | |
| $[A] = 1 + a_1 q^{-1} + a_2 q^{-2}$ | 1 | -1.871 | 0.871 | | | |
| $[A_m] = 1 + a_1 q^{-1} + a_2 q^{-2}$ | 1 | -1.429 | 0.4724 | | | |
| $[T] = t_0$ | 2.36 | | | | | |
| $[S] = s_0 + s_1 q^{-1}$ | 21.62 | -19.260 | | | | |
| $[R] = r_0 + r_1 q^{-1} + \cdots + r_{n_r} q^{-n_r}$ | 1 | 0.443 | 0.429 | 0.418 | 0.408 | -0.064 |

Table 6.1. Process models and control law parameters for left axis controller.

| Right Axis (Y2) | Pole-Placement Design Parameters | | | | | |
|---|---|---|---|---|---|---|
| $[B] = b_0 + b_1 q^{-1}$ | 982 | 505 | | | | |
| $[A] = 1 + a_1 q^{-1} + a_2 q^{-2}$ | 1 | -1.861 | 0.861 | | | |
| $[A_m] = 1 + a_1 q^{-1} + a_2 q^{-2}$ | 1 | -1.429 | 0.4724 | | | |
| $[T] = t_0$ | 2.85 | | | | | |
| $[S] = s_0 + s_1 q^{-1}$ | 21.07 | -18.225 | | | | |
| $[R] = r_0 + r_1 q^{-1} + \cdots + r_{n_r} q^{-n_r}$ | 1 | 0.398 | 0.373 | 0.352 | 0.335 | -0.076 |

Table 6.2. Process models and control law parameters for right axis controller.

## 6.3 Positioning System Performance

The equipment setup used for the performance experiments is depicted in figure 6.3. The object of these experiments was to evaluate the positioning system's performance in terms of dynamic response, position deadband, following error, tracking error and the effects of load force disturbance (compliance).
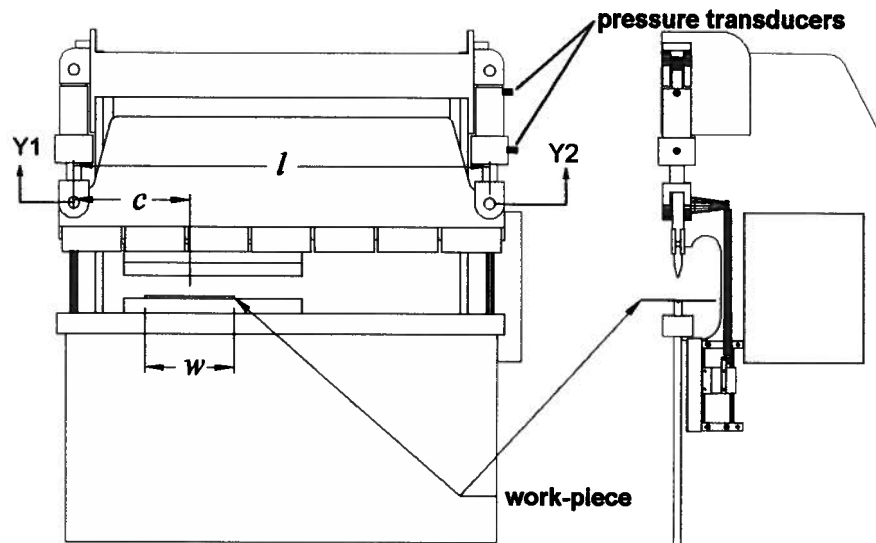
Figure 6.3. Press setup for positioning system performance experiments.

## 6.3.1 The Dynamic Response of the Ram Positioning System

A simple step response test was conducted to verify the dynamics response of each axis. For this test, each axis was given a reference command signal consisting a series of steps. The step amplitude was set as large as possible while avoiding controller saturation. The command signal and the measured position response are shown in figure 6.4. Negative steps represent actuator extension.

The results of this test indicate that rise time of each axis in extension (for this amplitude of excitation) is between 11 and 12 ms Furthermore, the extension response of each actuator exhibited no overshoot. The left actuator was observed to overshoot approximately 0 - 2% occasionally during retraction. This slight overshoot was deemed acceptable given that it does not occur during the forming operation. Moreover, the effect of any response overshoot would be mitigated somewhat by velocity profiling.
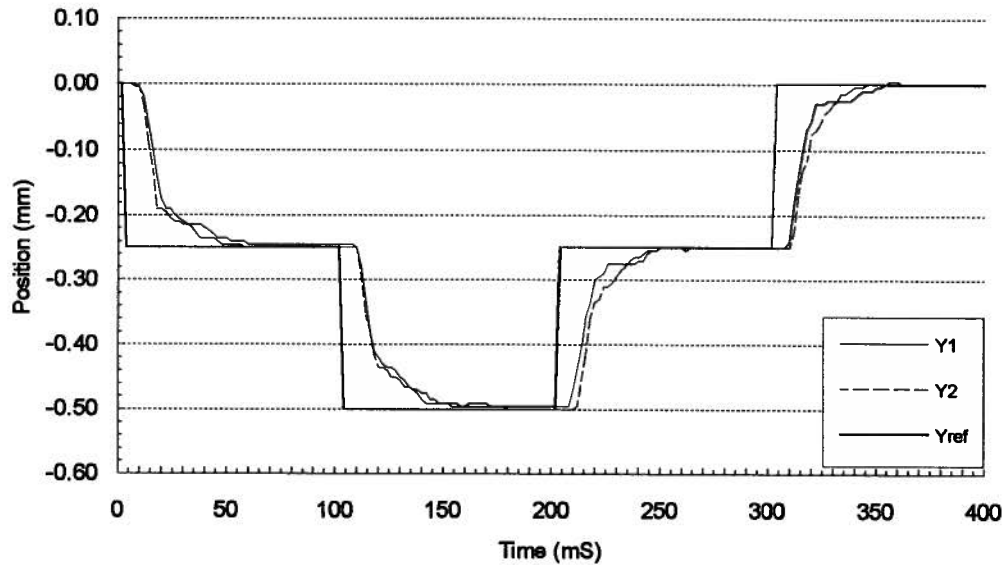
Figure 6.4. The response of left and right axis of the positioning system to a series of step changes in command position. Y1: left axis; Y2: right axis, Yref: reference command.

For comparison purposes, a traditional PID control algorithm was implemented and manually tuned. The response of the PID controlled system for one of the better tunings is shown in figure 6.5. From the following observations can be made:

- The rise time is between 20 and 30 ms

- Both axis exhibit between 6 and 9% overshoot during the extension and retraction.

- The settling time for each axis is greater than 300 ms

## 6.3.2 Determination of Positioning System Dead Band

The performance of hydraulic actuators is critically dependent on the performance of the valve. Valve hysteresis and spool stiction can cause excessive deadband in the positioning system. In order to determine the effects of these phenomena, each axis of the positioning system was given an alternating series of small steps in reference position. Both the reference and the actual axis positions were measured at two millisecond
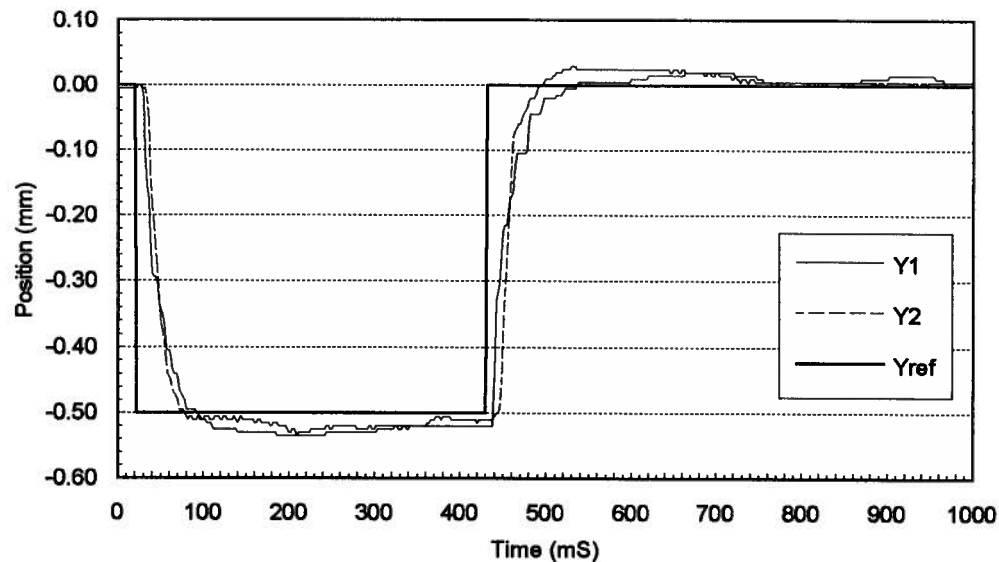
Figure 6.5. Response of PID controlled positioning system to step changes in reference position.

intervals. The results are presented in figure 6.6. These results indicate that the system deadband is smaller that one basic length unit (0.005 mm).

## 6.3.3 Determination of Controlled Motion Performance

One of the most important measures of a positioning system's performance is its ability to follow the desired motion profile. A measure of this following capability, the velocity error constant (VEC) is defined as the ratio of the following error to the desired velocity of the move. While the following error for either axis of the CNC press brake is not critical, the tracking error is, for this controls the orientation of the tooling. The tracking error will be proportional to difference between the VEC of each axis.

Hampering a press brake's ability to maintain constant tooling orientation is the tendency for the actuators to be unequally loaded. This occurs frequently because CNC press brakes are often used to perform a number of bends using a number of sets of
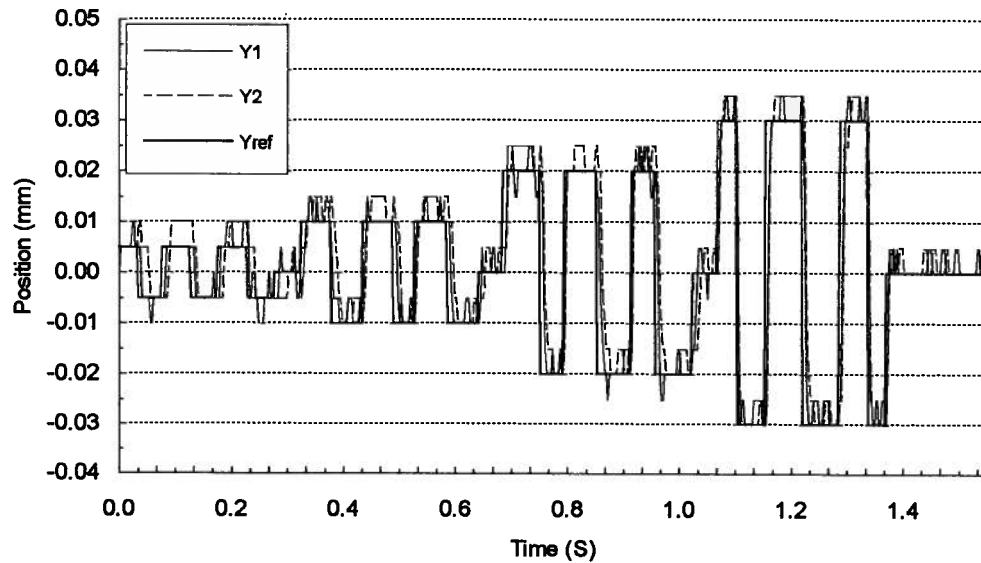
Figure 6.6. Response of positioning system to small changes in reference position.

tooling setup along the press bed. In the absence of coupling (be it mechanical, hydraulic, or controller coupling) between the axes, close axis tracking is achieved by matching the axis dynamics and ensuring both axes are stiff enough not to be affected significantly by disturbance loads.

In order to evaluate the performance of the positioning system with regards to these measures, two experiments were conducted. For the first experiment, a typical machine cycle motion profile was used to determine the VEC. For the second experiment, the same motion profile was used to perform a forming operations on several workpieces of differing geometry.

### 6.3.3.1 Motion Profile: No Forming Operation

The object of the motion profile experiment was to determine the ability of the positioning system to track the desired motion profile. For this experiment, each actuator was given a motion profile representing a typical bending operation: rapid approach, feed-

rate forming operation, dwell, and rapid retract. Sample results of this test are shown in figures 6.7 and 6.8. Note that the rough tracking response during the rapid move is due to an error in the linear interpolation routine. The velocity error constants for each axis are presented in table 6.3.

From these results the following observations can be made:

- The following error during the feed-rate move is less than 0.1 mm

- The velocity error constants for each of the axes are not equal. This is due to a slight mismatch of axis response times. Furthermore, for either axis, the VEC for extending case differs from that of the retracting case.

- The steady-state position error is not greater than 0.005 mm (one BLU) during the dwell operation.

- The relative position difference between each axis (the tracking error) is not greater than 0.015 mm (3 BLU) during the feed operation.

| Case: | Left Actuator VEC (ms) | Right Actuator VEC(ms) |
|---|---|---|
| Extension | 11.8 | 12.3 |
| Retraction | 13.4 | 11.9 |

Table 6.3. Velocity Error Constants for each axis as determined from motion profile tests: no forming loads.
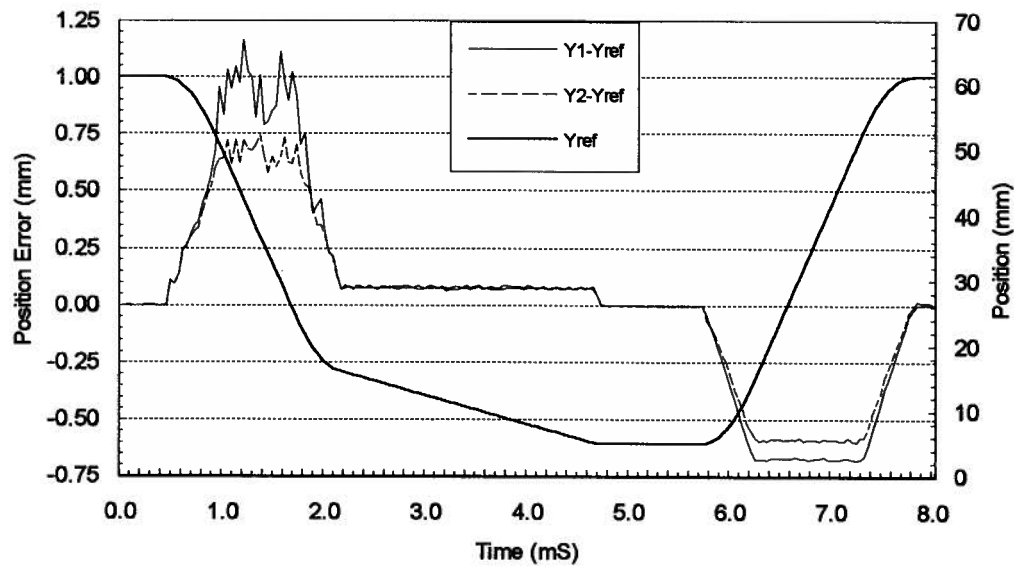
Figure 6.7. Response of positioning system to motion profile: no forming loads.
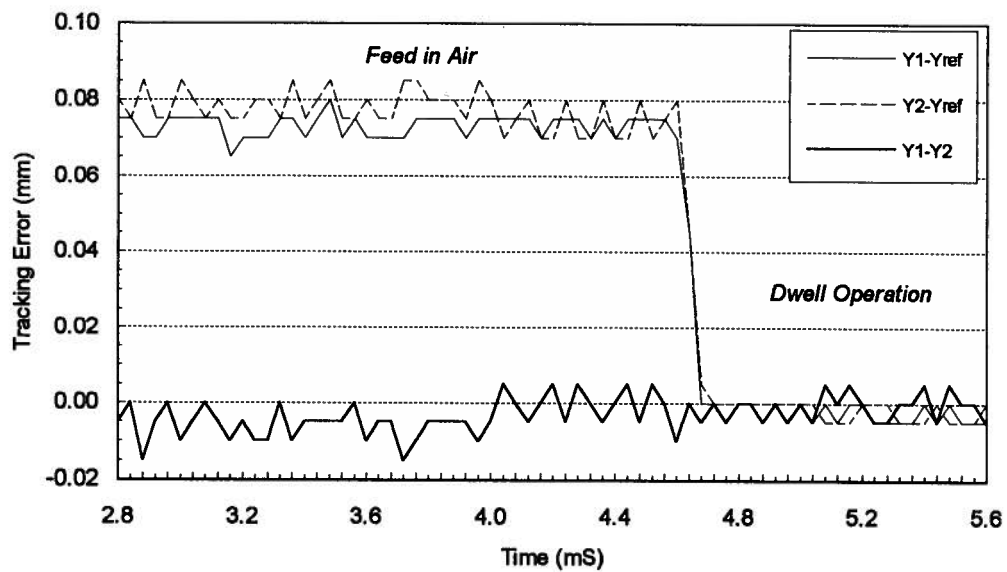


Figure 6.8. Plot of the absolute and relative tracking error of each positioning system: no forming loads.

## 6.3.3.2 Motion Profile: With Forming Operation

The object of this experiment was to determine the stiffness of the positioning system: that is, the ability to maintain tooling orientation and achieve the desired final punch penetration in the presence of typical forming loads. As with the previously described experiment, each actuator was given a motion profile representing a typical bending operation: rapid approach, feed-rate forming operation, dwell, and rapid retract. The tooling consisted of a 30 degree punch and a 90 degree die which were aligned and secured to the press. The respective centres of the punch and die were located 500 (mm) from the left actuator, (approximately 1/3 of the distance between the actuators) to allow asymmetrical actuator loading. Two pressure transducers, one for each fluid chamber, were installed in the right actuator. A typical work piece and the finished part are depicted in figure 6.9.

A series of tests were conducted forming workpieces of varying thicknesses and
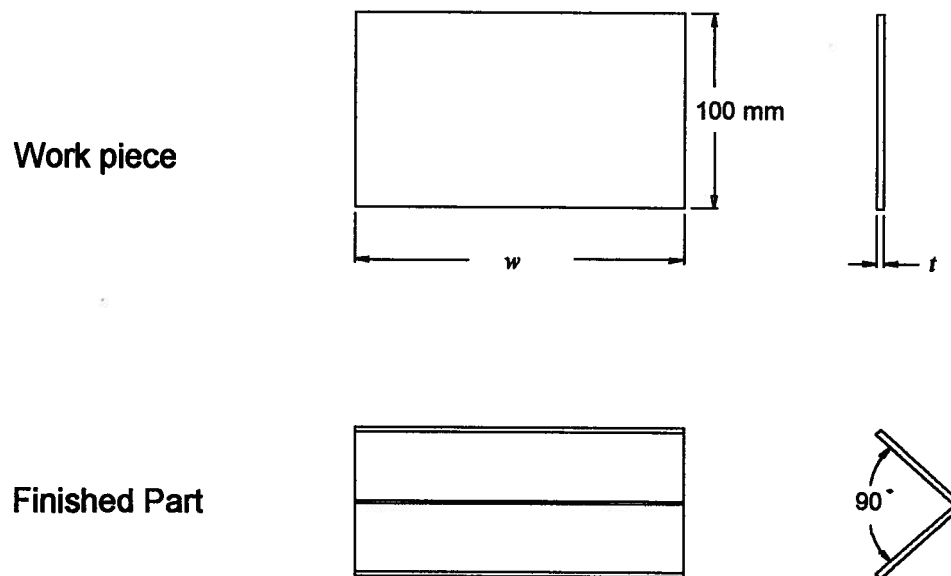


Figure 6.9. Sample work-piece and finished part used for brake-forming tests.

widths. The total width and geometric centre of the bend, $w$ and $c$ respectively, were recorded for each test. The hydraulic pressure acting in each chamber of the right actuator was measured as were the reference and actual positions of each axis during the bend cycle. Sample results of this test are shown in figures 6.10 and 6.11

Using the free body diagram shown in figure 6.12 the hydraulic pressure exerted by the right actuator was used to determine a static theoretical applied bending force distribution

$$F_b = \frac{R_{2y}l}{wc} \qquad \left[\frac{\text{kN}}{\text{m}}\right] \qquad (6.40)$$

as well as the force exerted by the left actuator for the dwell operation:

$$R_{1y} = R_{2y}\frac{l-c}{c} \quad [\text{kN}] \qquad (6.41)$$

The results of these test are shown in table 6.4

| Case | $w$ [mm] | $t$ [mm] | $c$ [mm] | $\dfrac{l-c}{l}$ | $y_1 - y_{ref}$ [$\mu$m] | $y_2 - y_{ref}$ [$\mu$m] | $R_{1y}$ [kN] | $R_{2y}$ [kN] | $F_b$ $\left[\text{kN/}_{\text{m}}\right]$ | $C_{1y}$ $\left[\frac{\mu\text{m}}{\text{kN}}\right]$ | $C_{2y}$ $\left[\frac{\mu\text{m}}{\text{kN}}\right]$ |
|------|------|------|------|------|------|------|------|------|------|------|------|
| 1 | 150 | 1.5 | 425 | 0.70 | 4 | 5 | 7.1 | 3.0 | 67 | 0.50 | 1.81 |
| 2 | 300 | 1.5 | 500 | 0.65 | 9 | 12 | 13.5 | 7.3 | 69 | 0.64 | 1.62 |
| 3 | 600 | 1.5 | 500 | 0.65 | 13 | 15 | 29.9 | 16.2 | 77 | 0.44 | 0.92 |
| 4 | 150 | 3.0 | 725 | 0.49 | 13 | 38 | 26.5 | 27.6 | 360 | 0.47 | 1.38 |
| 5 | 200 | 3.0 | 700 | 0.51 | 24 | 47 | 41.4 | 40.2 | 408 | 0.59 | 1.17 |
| 6 | 200 | 3.0 | 700 | 0.51 | 21 | 51 | 42.7 | 41.4 | 421 | 0.50 | 1.24 |

Table 6.4. Results of the Brake forming analysis.

Note: the computation of the axis compliance values presented in table 6.2 is based on an assumption that the entire positioning error is due to the disturbance load. The results of the previous section indicate that up to 4 to 5 $\mu$m of positioning error exists regardless of disturbance loads. Therefore, the axis compliance values determined for relatively low load forming conditions may be somewhat overestimated. Given this, the

compliances of the left and right axis, averaged for the four larger bending loads were determined to be:

$$C_{1y} = 0.50 \left[ \frac{\mu m}{kN} \right] \tag{6.42}$$

$$C_{2y} = 1.18 \left[ \frac{\mu m}{kN} \right] \tag{6.43}$$

Based upon the system pressure and the piston area, an upper bound on the force capacity of each actuator was determined to be 50 [kN]. Considering the reduction in valve gain due to pressure drop, a practical bound on the actuator capacity should be much lower.
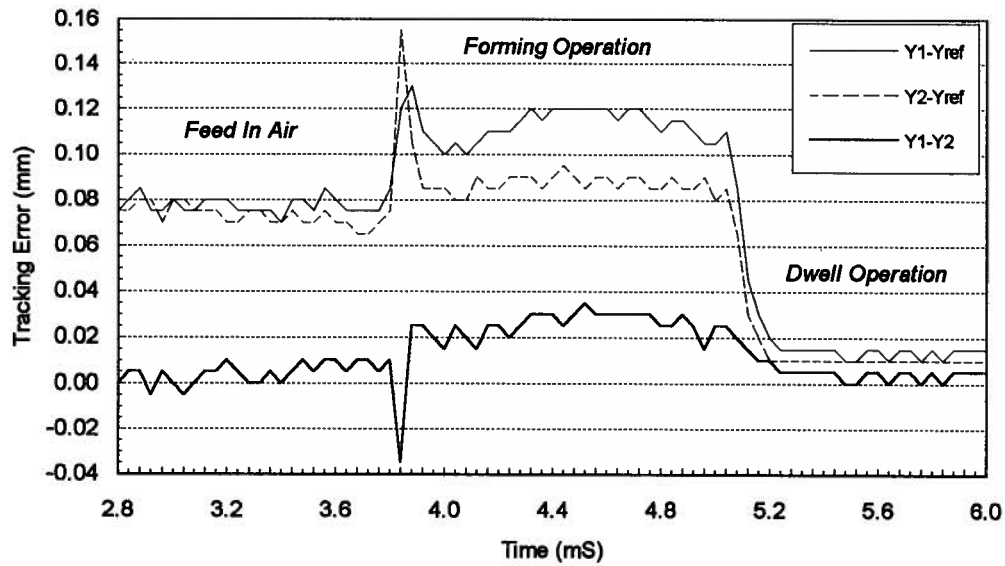
Figure 6.10. Plot of the absolute and relative tracking error of each positioning system: Motion profile with bending operation.
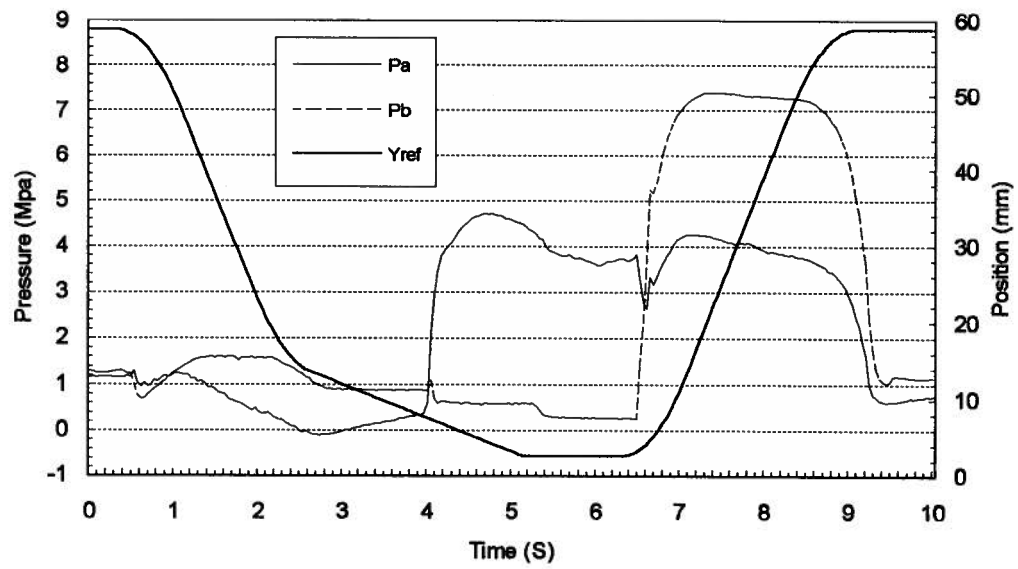
Figure 6.11. Actuator pressures recorded for motion profile with forming operation.
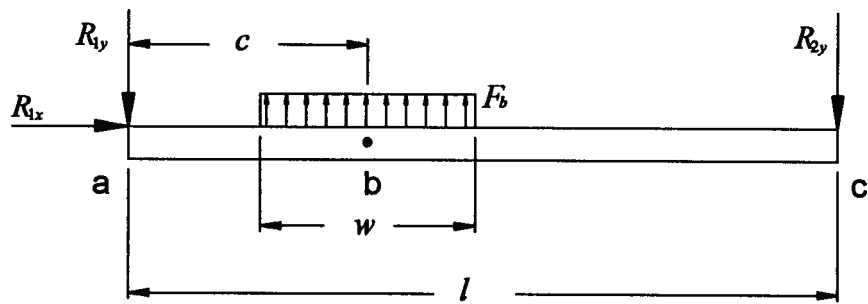


Figure 6.12. Free-body diagram of forces acting on ram during the dwell operation.

## 6.4 Conclusions

In this chapter, details of the control scheme were presented. A practical simplification to the pole-placement control law was developed and implemented. The performance of the positioning system can be summarized as follows:

- The rise time of the response of the positioning system to a step change in position was 11-12 ms for each axis.

- The dead-band was found to be less than one basic length unit (BLU=0.005mm).

- The steady-state positioning error (under no load) was found to be less than one BLU.

- The compliance of each axis of the positioning system was determined to be:

$$\text{Left axis (Y1): } 0.50 \left[ \frac{\mu\text{m}}{\text{kN}} \right]$$

$$\text{Right axis (Y2): } 1.18 \left[ \frac{\mu\text{m}}{\text{kN}} \right]$$

# Chapter 7

# Conclusions and Recommendations

In this thesis a computer-controlled positioning system for a hydraulic press brake was designed, modeled and analyzed. Both linear and non-linear system models were applied to cylindrical hydraulic actuators. Non-linear state-relations describing the change in actuator compliance with position were developed. An analysis of the actuator system dynamics was conducted using a variety of models. The results indicate that simple linear models are capable of predicting the dynamic mode of an asymmetrical actuator if the valve flow coefficients are known. However, the piston position and the direction of piston movement during critical positioning stages also need to be considered in system design.

Hydraulic components for the system supply and servo-actuator were chosen and implemented.

The gibbing of the press-brake was modified to allow rotation in the plane of the ram. A position feedback system was designed, implemented and tested. No backlash was detected.

Experiments were conducted to determine the system dynamics of the hydraulic servo-actuators. Step response and frequency response tests indicate a first order model with consideration of delay is acceptable. Dynamic system parameters were determined using parametric identification techniques.

A delay-compensating, pole-placement control law was designed for the model structures determined in the identification section. A universal simplification of the pole-placement control law for processes with inherent integration was developed and

implemented. This simplification eliminated output scaling errors while also reducing computational overhead. Motion profile tests indicated that dynamics of each axis were adequately matched. Also, the system exhibited less than one basic length unit steady-state position error on a positioning move. Actuator compliances were determined for each axis through actual bending tests.

In order to create a satisfactory position system, this work has effectively outlined a procedure for designing position control systems for CNC press-brakes. With regard to this procedure, future work needs to be conducted in identification and control. For this thesis, all identification experiments were carried out in open-loop. While this was relatively safe for this small press, it could be quite dangerous for much larger ones. Closed-loop identification techniques should be investigated.

For improved motion control, integrating pole-placement controllers could be used to enhance the stiffness of the positioning system if numeric sensitivity and valve irregularities were overcome. Also, cross-coupled control strategies should be examined as a means of reducing axis tracking errors.

Finally, since the stiffness of hydraulic actuators is adversely affected by dissolved gases in the fluid a system for determining the bulk modulus of a samples of fluid would be a tremendous asset.

# BIBLIOGRAPHY

1. Pourboghrat, F. and Stelson, K.A., "Pressbrake Bending in the Punch-Sheet Contact Region-Part 1: Modeling Nonuniformities", Trans. of ASME, J. Eng. for Ind., Vol.110, pp125-130, 1988.

2. Anon. "Sheet Metal Bending Methods", Accurate Manufacturing Company News Release, EM-105.

3. Anon. "Bottom Bending", Accurate Manufacturing Company News Release, EM-106.

4. Vaccari, John, "CNC Press Brakes", American Machinist, pp57-64, August, 1989.

5. Anon., "Bend Allowance", Accurate Manufacturing Company News Release, EM-108.

6. Abo-Ismail, A. and Ray, A., "Effect of Non-linearities On The Transient Response of an Electrohydraulic Position Control Servo", Journal of Fluid Control, Vol. 17, No. 3, pp59-79, ??.

7. Ashley, C. and Mills, B., "Frequency Response of an Electro-hydraulic Vibrator with Inertial Load", Journal of Mechanical Engineering Science, Vol. 8, No. 1, pp27-35, 1966.

8. Davies, A. M. and Davies, R. M., "Non-linear Behavior, Including Jump Resonance, of Hydraulic Servomechanisms", Journal of Mechanical engineering Science, Vol. 11, No. 3, 1969.

9. Gale, P. and Bell, R., "An Economic Technique For The Improvement of the Stability of Hydraulic Cylinder Drives", Proceeding of the Twelfth International Machine tool Design & Research Conference, pp207-216, 1971.

10. Guillon, M. and Blondel, J. P., "Non-symmetrical Cylinders and Valves Under Non-symmetrical Loading", Second Fluid Power Symposium, B5, pp85-99, 1971.

11. Martin, K. F., "Stability and Step Response of a Hydraulic Servo with Special Reference to Unsymmetrical Oil Volume Conditions", Journal of Mechanical engineering Science, Vol. 12, No. 5, pp331-338, 1970.

12. Martin, K. F., "Flow Saturated Step Response of a Hydraulic Servo", Trans. of ASME, Journal of Dynamic Systems Measurement and Control, Vol.??, pp341-346, 1974.

13. McLoy, D. and Martin, H. R., *The Control of Fluid Power*, John Wiley & Sons, New York, 1990.

14. Merritt, H., E., *Hydraulic Control Systems*, John Wiley & Sons, New York, 1967.

15. Royle, J. K., "Inherent Non-linear Effects in Hydraulic Control Systems with Inertia Loading", Proc. Instn. Mech. Engrs. Vol. 173, No. 9, pp257-269, 1959.

16. Watton, J., "The Generalized Response of Servovalve-Controlled, Single-Rod, Linear Actuators and the Influence of Transmission Line Dynamics", Trans. of ASME, Journal of Dynamic systems Measurement and Control, Vol.106, pp157-162, 1984.

17. Bell, R. and de Pennington, A., "Active Compensation of Lightly Damped Electrohydraulic Cylinder Drives Using Derivative Signals", Proc. Instn Mech. Engrs., Vol. 184, Pt. 1, No. 4, pp83-98, 1969.

18. Shearer, J. L., "Digital Simulation of a Coulomb-Damped Hydraulic Servosystem", Journal of Dynamic Systems Measurement and Control, Vol. 105, pp215-221, 1983.

19. Bell, R., "The Use of Hydraulic Drives on N.C. Machine Tools -- A Re-Evaluation", International Journal of Machine Tool Design and Research, Vol. 11, pp209-222, 1971.

20. Edge, K. A. and Figueredo, K. R. A., "An adaptively controlled electrohydraulic servo-mechanism. Part 1: adaptive controller design", Proc. Instn. Mech. Engrs., Vol. 201, No. B3, pp175-180, 1987.

21. Lambert, T. H. and Davies, R. M., "Investigation of the Response of an Hydraulic Servomechanism with Inertia Load", Journal of Mechanical engineering Science, Vol. 5, No. 3, pp281-294, 1963.

22. Watton, J.,"A Digital Compensator Design for Electrohydraulic Single-Rod Cylinder Position Control Systems", Trans. of ASME, Journal of Dynamic systems Measurement and Control, Vol.112, pp403-409, 1990.

23. Lee, S. R. and Srinivasan, K., "Self-tuning Control Application to Closed-Loop Servohydraulic Material Testing", Trans. of ASME, Dynamic Systems, Measurement, and Control, Vol. 112, pp681-689, 1990.

24. Takahashi, K. and Takahashi, Y., "Dynamics Characteristics of A Spool-valve-controlled Servomotor with a Non-symmetrical Cylinder", Bulletin of the JSME, Vol. 23, No. 181, pp1155-1162, 1980.

25. Daley, S., "Application of a fast self-tuning control algorithm", Proc. Instn. Mech. Engrs., Vol. 200, No. C6, pp425-430, 1986.

26. Anon, Atchley 320 Technical Information, 1991.

27. Newell, N. A., "Implementation of a Hierarchical Open Architecture Multiprocessor Computer Numerical Controller", Graduate Thesis, The University of British Columbia, 1993.

28. Neal, T. P., "Performance Estimation for Electrohydraulic Control Systems", Moog Technical bulletin, No. 126, 1974.

29. Watton, J., "Further contributions to the Response and Stability of Electrohydraulic Servo Actuators with Unequal Areas - Part 1, System Modelling.", Proc. ASME Winter Annual Meeting, 1985

30. Anon., "*Parker Hydraulic Products and Total Systems Engineering: Catalogue 0108*", Parker Hannifin Corporation.

31. Parker, G. A. and Desjardins, Y. C., "A Comparison of Transfer Function Identification Methods for an Electro-hydraulic Speed Control System", Third International Fluid Power Symposium, Paper E2, pp1-27, 1973.

32. Soderstrom, T. and Stoica, P., *System Identification*, Prentice Hall Inc., 1989.

33. Anon., *Matlab Reference Guide*, The Mathworks Inc., 1992.

34. Astrom, K.,J. and Wittenmark, B., *Computer Controlled Systems*, Prentice-Hall, Inc., 1984.

# APPENDIX A

## Actuator Natural Frequency Calculations

An estimate of the natural frequency of the actuator is provided by equation 4.28:

$$\omega_l = \sqrt{\frac{4\beta_e A_p^2}{V_t M_r}} \qquad\qquad \text{A.1}$$

Given:

| | | |
|---|---|---|
| Half mass of ram: | $M_r = 104$ | [kg] |
| Cap side piston area: | $A_p = 0.00456$ | [m$^2$] |
| Rod side piston area: | $A_r = 0.00253$ | [m$^2$] |
| Total actuator fluid volume at the most compliant position: | $V_t = 455e^{-6}$ | [m$^3$] |
| Bulk modulus of fluid: | $\beta_e = 689.5e^6$ | [N/m$^2$] |

Using the average piston areas to accommodate for actuator asymmetry:

$$\omega_l = \sqrt{\frac{4(689.5e^6)\left(\dfrac{0.00456+0.00253}{2}\right)^2}{(455e^{-6})(104)}}$$

$$\omega_l = 860 \text{ [rad/s]}$$

or,

$$f_l = 137 \text{ [Hz.]}$$

# APPENDIX B

## Derivation of Pole-Placement Control Law Parameters

For a system with an open-loop position response characterized by the discrete-time transfer function:

$$\frac{y(q)}{u(q)} = \frac{B(q)}{A(q)} = \frac{b_1 q^{n_b} + b_2 q^{n_b-1} + \cdots + b_{n_b+1}}{q^{n_d}\left(q^{n_a} + a_1 q^{n_a-1} + \cdots + a_{n_a}\right)}, \tag{B.1}$$

choose a desired closed-loop system response which has the same order and the same number of delays:

$$\frac{y(q)}{y_{ref}(q)} = \frac{B_m(q)}{A_m(q)} = \frac{(b_1 q + b_2) b_{m0}}{q^{n_d}\left(a_{m0} q^{n_a} + a_{m1} q^{n_a-1} + \cdots + a_{m(n_a)}\right)} \tag{B.2}$$

where $a_{m_0} = 1$. For a unity gain system,

$$b_{m0} = \frac{1 + \sum\limits_{i=1,n_a} a_{m_i}}{\sum\limits_{j=1,n_b+1} b_j} \tag{B.2}$$

In order for the controller to be causal, the order of the observer polynomial must satisfy the following constraint:

$$\deg A_0(q) \geq 2\deg A(q) - \deg A_m(q) - 1 \tag{B.2}$$

$$\deg A_0(q) \geq 2(n_a + n_d) - (n_a + n_d) - 1$$

$$\deg A_0(q) \geq n_a + n_d - 1$$

If the control law takes a relatively small amount of time to implement we are free to choose:

$$\deg A_0(q) = n_a + n_d - 1 \qquad \text{B.2}$$

For low-noise transducers such as optical encoders, it is desirable to place the observer polynomials at the origin for the fastest response such that:

$$A_0 = q^{n_a + n_d - 1} \qquad \text{B.2}$$

The order of the controller poles must be such that:

$$\deg R(q) \geq \deg A_0(q) + \deg A_m(q) - \deg A(q)$$

$$\deg R(q) \geq (n_a + n - 1_d) + (n_a + n_d) - (n_a + n_d)$$

$$\deg R(q) \geq n_a + n - 1_d$$

Again, if the controller output signal happens near the beginning of the loop closure cycle, we are free to choose:

$$\deg R(q) = \deg S(q) = n_a + n - 1_d$$

such that:

$$R(q) = r_0 q^{n_r} + r_1 q^{n_r - 1} + \cdots + r_{n_r} \qquad \text{B.2}$$

$$S(q) = s_0 q^{n_r} + s_1 q^{n_r - 1} + \cdots + s_{n_r} \qquad \text{B.2}$$

where:

$$n_r = n_a + n_d - 1$$

The feed-forward filter is chosen:

$$T(q) = b_{m0} A_0 = b_{m0} q^{n_r} \qquad \text{B.2}$$

In determination of the control law coefficients requires the solution of the Diophantine equation:

$$A(q)R(q) + B(q)S(q) = A_0(q)A_m(q)$$

Expanding B.9:

$$q^{n_d}\left(a_0 q^{n_a} + a_1 q^{n_a - 1} + \cdots + a_{n_a}\right)\left(r_0 q^{n_r} + r_1 q^{n_r - 1} + \cdots + r_{n_r}\right) +$$

$$\left(b_1 q^{n_b} + b_2 q^{n_b - 1} + \cdots + b_{n_b + 1}\right)\left(s_0 q^{n_r} + s_1 q^{n_r - 1} + \cdots + s_{n_r}\right) = q^{n_r} q^{n_d}\left(q^{n_a} + a_{m_1} q^{n_a - 1} + \cdots + a_{m_{n_a}}\right) \qquad \text{B.10}$$

For $n_a = 2$, $n_b = 1$, $n_d > 1$ collecting terms of B.10 of like orders yields:

$$q^{2(n_a+n_d)-1}: \quad a_0 r_0 \qquad\qquad\qquad =1 \qquad\qquad\qquad \text{B.11}$$

$$q^{2(n_a+n_d)-2}: \quad a_0 r_1 + a_1 r_0 \qquad\qquad =a_{m_1} \qquad\qquad \text{B.12}$$

$$\vdots \quad \vdots \qquad\qquad\qquad\qquad \vdots$$

$$q^{n_a+n_d}: \quad a_0 r_{n_r} + a_1 r_{n_r-1} + a_2 r_{n_r-2} + b_1 s_0 \quad =0 \qquad \text{B.13}$$

$$q^{n_a+n_d-1}: \quad a_1 r_{n_r} + a_2 r_{n_r-1} + b_1 s_1 + b_2 s_0 \quad =0 \qquad \text{B.14}$$

$$q^{n_d}: \quad a_2 r_{n_r} + b_1 s_2 + b_2 s_1 \quad =0 \qquad \text{B.15}$$

$$q^{n_d-1}: \quad b_1 s_3 + b_2 s_2 \quad =0 \qquad \text{B.16}$$

$$\vdots \qquad\qquad\qquad\qquad \vdots \quad \vdots$$

$$q^1: \quad b_1 s_{n_d+1} + b_2 s_{n_d} \quad =0 \qquad \text{B.17}$$

$$q^0: \quad b_2 s_{n_d+1} \quad =0 \qquad \text{B.18}$$

Assuming $b_1 \neq 0$ and $b_2 \neq 0$, solving B.17 and B.18 yields:

$$s_{n_d+1} = 0 \qquad\qquad\qquad\qquad \text{B.19}$$

$$s_{n_d} = 0 \qquad\qquad\qquad\qquad \text{B.20}$$

Back substituting into the series of equations inferred between B.15 and B.17 we can determine that:

$$s_2 : s_{n_d-1} = 0 \qquad\qquad\qquad \text{B.21}$$

Solving B.13 for $s_0$:

$$s_0 = -\frac{\left( a_0 r_{n_d+1} + a_1 r_{n_d} + a_2 r_{n_d-1} \right)}{b_1} \qquad \text{B.22}$$

Solving B.15 for $s_1$:

$$s_1 = -\frac{a_2 r_{n_d+1}}{b_2} \qquad\qquad\qquad \text{B.23}$$

Solving B.11 - B.13 yields:

$$r_0 = 1 \tag{B.24}$$

$$r_1 = a_{m_1} - a_1 \tag{B.25}$$

$$r_2 = a_{m_2} - a_2 - a_1 r_1 \tag{B.26}$$

$$r_i = -(a_2 r_{i-2} + a_1 r_{i-1}), \qquad i = [3:n_d] \tag{B.27}$$

Solving B.22 and B.23 into B.14 and solving for $r_{n_d+1}$ yields:

$$r_{n_d+1} = \frac{a_1 r_{n_d} \dfrac{b_2}{b_1} + a_2 \left( r_{n_d-1} \dfrac{b_2}{b_1} - r_{n_d} \right)}{a_1 - a_2 \dfrac{b_1}{b_2} - \dfrac{b_2}{b_1}} \tag{B.27}$$

# APPENDIX C

## Friction Characteristics of Guide System

The contribution of the guide system was measured for a variety of actuator speeds. The results are presented in figure C.1
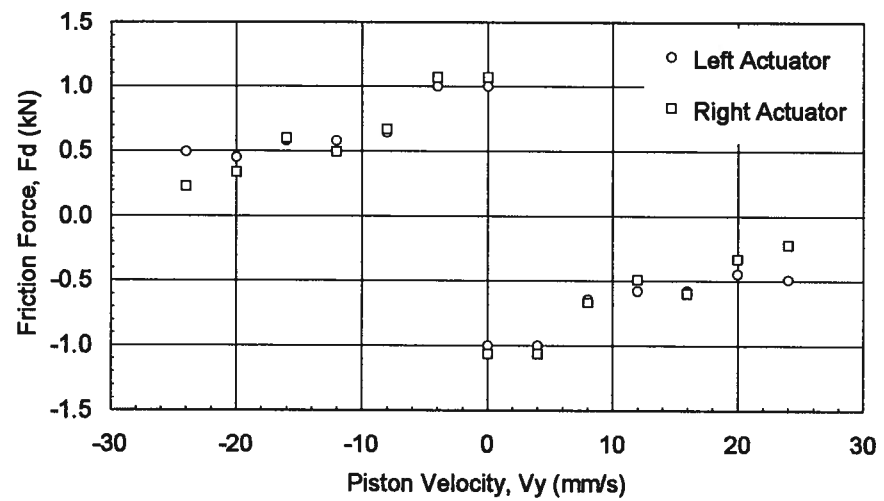


Figure C.1. Friction force exerted by guide system.

# APPENDIX D

## Model Parameters

$M_r = 104$     [kg]

$B_r = 0$     $[\mathrm{N \cdot s/m}]$

$A_p = 0.00456$     $[\mathrm{m}^2]$

$A_r = 0.00253$     $[\mathrm{m}^2]$

$V_t = 455e^{-6}$     $[\mathrm{m}^3]$

$\beta_e = 689.5e^6$     $[\mathrm{N/m}^2]$

$V_{al} = 20.56e\text{-}6$     $[\mathrm{m}^3]$;

$V_{bl} = 35.05e\text{-}6$     $[\mathrm{m}^3]$;

$K_c = 6.04e\text{-}6$     $\left[\mathrm{m}^5/\mathrm{N \cdot s}\right]$

$K_{lp} = 0$     $\left[\mathrm{m}^5/\mathrm{N \cdot s}\right]$

$K_{le} = 0$     $\left[\mathrm{m}^5/\mathrm{N \cdot s}\right]$

$K_q = 144.6e\text{-}6$     $\left[\mathrm{m}^3/\mathrm{s}\right]$

$L = 0.125$     [m]

$F_c = (300,600)$     [N]

$p_s = 690$     [Mpa]

$p_t = 0$     [Mpa]

$\tau_v = 0.005$     [ms]

$g = 9.81$     $\left[\mathrm{m/s}^2\right]$